Fall 2020

Development of amine-functionalized mesoporous alumina for radioiodine removal from water

Mansour Mohammed Alsalbokh

Department:

DEVELOPMENT OF AMINE-FUNCTIONALIZED MESOPOROUS ALUMINA FOR RADIOIODINE REMOVAL FROM WATER

by

MANSOUR MOHAMMED ALSALBOKH

A THESIS

Presented to the Graduate Faculty of the

MISSOURI UNIVERSITY OF SCIENCE AND TECHNOLOGY

In Partial Fulfillment of the Requirements for the Degree

MASTER OF SCIENCE IN CHEMICAL ENGINEERING

2020

Approved by:

Ali Rownaghi, Advisor
Fateme Rezaei
Douglas Ludlow

PUBLICATION THESIS OPTION

This thesis consists of the following two articles, formatted in the style used by the Missouri University of Science and Technology:

Paper I, found on pages 15-37, is intended for submission to the *Chemical Engineering Journal*.

Paper II, found on pages 38-53, is intended for submission to the *Chemical Engineering Journal*.

ABSTRACT

Radioactive materials have spread due to careless disposal and nuclear disasters. Some radionuclides can exist in an aqueous media, like radioactive iodine. As a result, in this work amine-functionalized mesoporous alumina was developed to adsorb radioactive iodine from the liquid phase. Bismuth was incorporated, using a wet impregnation method, to test it as a possible silver replacement. Amine grafting was used to functionalize the surface of the mesoporous alumina. All materials prepared in this work were characterized by N_2 physisorption, FTIR and TGA to determine the textural properties, surface functionality, and amine loading. The synthesized materials were tested for iodine adsorption in batch experiments. The effect of initial iodine concentration, temperature, contact time, bismuth loading, amine chain, and amine loading were studied in this work. The iodine adsorption capacities were obtained, and it was found that Bi_{15}/Al-DMAPS had the highest iodine adsorption capacity of 215 mg/g in the first paper; whereas, Al-DMAPS had the highest iodine adsorption capacity of 241 mg/g in the second paper. BET surface areas were also obtained and found to be 176 and 191 m^2/g for Bi_{15}/Al-DMAPS and Al-DMAPS, respectively.

ACKNOWLEDGMENTS

I would like to express my deepest gratitude for my advisor, Dr. Ali Rownaghi, for his guidance, advice, and patience. His support and trust played a very important role in building and developing my research skills. My appreciation goes to my committee members, Dr. Fateme Rezaei, for allowing me to use her instruments and trusing me with her projects and Dr. Ludlow for his support.

I thank my sponsor, the Saudi Arabian Culture Mission (SACM), for the financial support during my academic study. I would like to thank my teammates who helped me to achieve this.

Finally, I would like to express a big thank you to my family and friends in Saudi Arabia and in the US for their continuous support and you having faith in me. I would not have done this without them.

TABLE OF CONTENTS

Page

LIST OF ILLUSTRATIONS

PAPER II

LIST OF TABLES

NOMENCLATURE

Symbol	Description
γ	The phase of crystalline structure

1. INTRODUCTION

1.1. RADIOACTIVE WASTES

Radioactive materials have gained popularity in several fields. Radioactive materials have been used for diagnosing and treating diseases, producing energy, tracing industrial applications, and for other purposes.[1–3]. For power generation, nuclear power plants have been proven to be the most efficient and cleanest power generating method, hence nuclear power plants are popular[4]. According to a 2011 study, 14% of the world's electricity was produced by nuclear power plants[5]. Despite the advantages of nuclear power generation, there are critical drawbacks. Nuclear power generation is more favorable than the tradition combustion methods because it produces less wastes; however, nuclear wastes are substantially more dangerous than the wastes produced by combustion[2]. Up to now, there has not been any solutions to dispose of with radioactive wastes, except storing them[2]. Radioactive iodine (RI) is one of the nuclear wastes, and it is produced as a result of the fission reaction of uranium[6]. RI exist in two forms: ^{131}I that has a half-life of 8 days and ^{129}I that has a half-life of 15 million years[4,7]. The fact that RI can exist as a gas or in water means that the soil, farm products, and dairy products have the potential to be contaminated, which makes it a serious concern[6]. Furthermore, during accidents, water with radioactive contaminant -RI included- leak from the reactors to the environment[8]. The Fukushima and the Chernobyl accidents caused radioactive contaminants to spread in soil, ground water, and aquatic environments[9,10].

1.2. HEALTH EFFECTS

Radio therapy is one of the treatment methods used commonly to treat some types of cancers, like thyroid cancer [11,12]. Radio therapy doses are very precise and target the cancer cells. Conversely, being exposed to radiation after an accident in a nuclear power plant (NPP) or an atomic bomb explosion subjects the entire body to high doses [13]. Radiation can cause damage to the DNA, which results in mutations [14]. Damaged DNA may also send signals stimulating cell growth that cause cancers [14]. ^{129}I and ^{131}I are believed to cause thyroid cancer and leukemia [15].

2. LITERATURE REVIEW

The main focus of this work is removing radioactive iodine from the liquid phase using aluminum-oxide. Aluminum-oxide, or alumina, is almost exclusively used by the chemical industry in the catalysis and separation fields for adsorption applications. Alumina and its variations have been studied extensively for CO_2 capture[16–22]. Transition aluminas or aluminum-oxides synthesized form boehmite were classified into three main polymorphs: γ-Al_2O_3, δ-Al_2O_3, and θ-Al_2O_3. For the structures, θ-Al_2O_3 is very well documented [23,24]. At the structural level, all three phases have the O atoms in a packed cubic structure [24,25]. The phases differ in the Al atom distribution on the octahedral and tetrahedral positions. Furthermore, γ-Al_2O_3 is described as a defective cubic spinal structure [24]. This literature review thoroughly discusses the methods that have been investigated for iodine adsorption in the gas and liquid phases. Moreover, previous work in iodine adsorption via alumina is reviewed.

2.1. IODINE ADSORPTION

Iodine under normal conditions at room temperature is solid, but with heat it vaporizes (sublimation)[26]. As a result of that, iodine can exist as a vapor or dissolved in liquids[27]. This section reviews some of the methods listed in the literature and used to adsorb or remove iodine from a gas phase or liquid phase.

2.1.1. Gas Phase. Some of the types of iodine adsorbents in the gas phase are: Porous Organic Frameworks (POFs), silver-based materials, and wet scrubbing. The

following sections discuss some of the highlights and improvements that have been made in this area during the last decade.

2.1.1.1. POFs. Metal-organic frameworks or MOFs are three-dimensional crystalline porous structures connected by a net of metal ions [28]. The crystallinity of the MOFs, the super high surface area, the tunability, and the ability to be used at an industrial scale make MOFs attractive [29]. Metal-organic frameworks development field is probably one of the most crowded fields in the last decade. It has been tested for several applications, like catalysis, separation, and conductivity. [29–34]. Commercial HKUST-1 from Sigma Aldrich (Figure 2.1) with a high surface area of 1500-2100 m^2/g was tested for iodine adsorption with 3.5% relative humidity, ambient pressure, and at 75 ^oC. The research group reported 175 wt % iodine adsorption capacity [35]. Another group tested porous aromatic frameworks (PAF) PAF-23, PAF-24, and PAF-25 (Figure 2.2) with a surface areas of 82, 136, and 262 m^2/g, respectively. At 75 ^oC and with ambient pressure, PAF-23, PAF-24, and PAF-25 had iodine adsorption capacities of 271, 276, and 260 wt %, respectively [36]. Conjugated microporous polymers (CMPs) have also been studied for iodine adsorption. It is novel approach of two CMPs modified by polymerization with thiophene monomers (Figure 2.3) that make the structure electron-rich which, as a result, improve the adsorption capacity [37,38]. This combination resulted in an iodine adsorption capacity of 345 wt % [38]. Kongzhao Su synthesized and tested an array of novel calix [4] resorcinarene-based porous organic frameworks (CalPOFs), which were prepared by diazocoupling reaction coupling [39]. CalPOF-1, which has a surface area of 303 m^2/g, had an iodine adsorption capacity of 477 wt % [39]. Guo et al. reported the highest iodine capacity of 543 wt % [40]. Porous organic polymers (POPs) have also contributed to this field. In one study, Geng and

coworkers synthesized biimidazole (BIM)-based POPs and then functionalized them with 2,4,6-trichloro-1,3,5-triazine (TCT) and hexa- chlorocyclotriphosphazene (HCCP) to make TBIM and HBIM, respectively [41]. Despite the poor textural properties of TBIM and HBIM (BET surface area of 8.12 and 5.27 m^2/g, respectively), TBIM and HBIM had an iodine adsorption capacities of 9.43 and 8.11 g/g, respectively, which is the highest iodine capacities recorded at the time of writing this review. The high iodine adsorption capacities were attributed to the willingness of those adsorbents to donate electrons to the electron deficient iodine ion [41]. Table 2.1. summarizes the properties, capacities and conditions of these results.

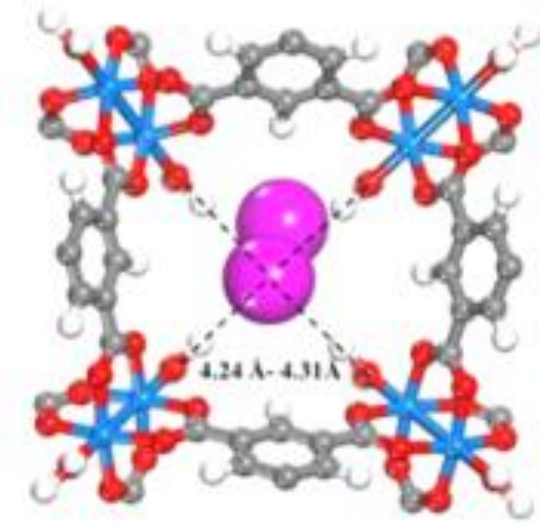

Figure 2.1. I_2-MOF entrapment from a four ring window. Atoms' color: purple = I, blue = Cu, gray = C, red = O, and white = H.

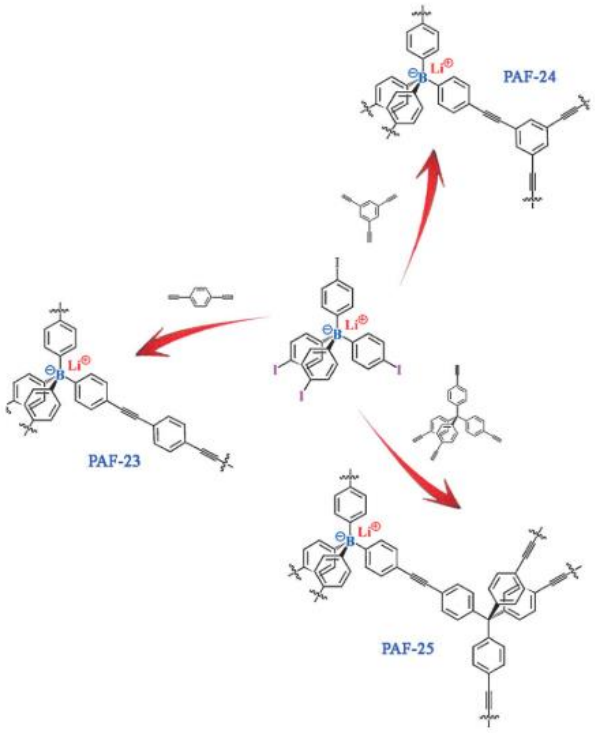

Figure 2.2. Synthesis routes for PAF-23, PAF-24, and PAF-25.

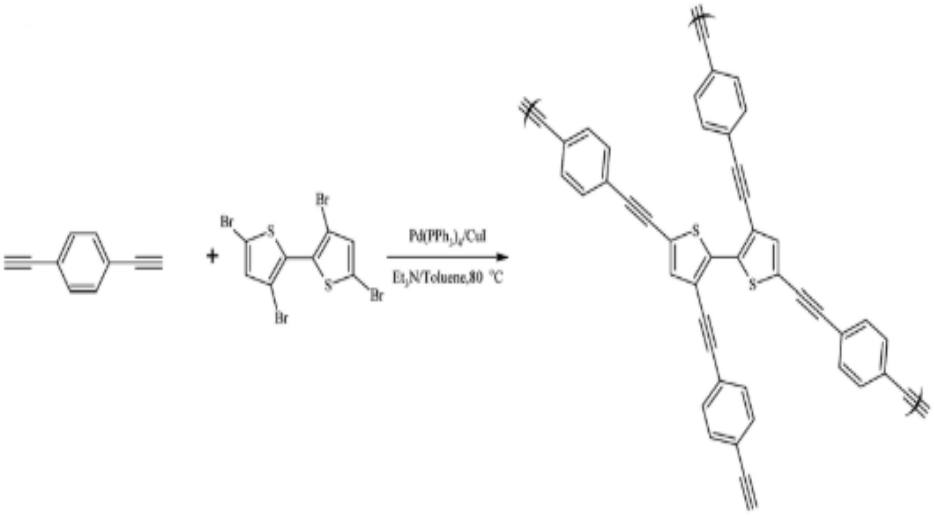

Figure 2.3. The structure of CMP-II polymerize with thiophene.

Table 2.1. I_2 captured by POFs.

Material	S_{BET} (m^2/g)	Iodine capture capacity (wt %)	Conditions	Ref.
HKUST-1	1500-2100	175	75 °C, 1 bar, 3.5% RH	[35]
PAF-23	82	271	75 °C	[36]
PAF-24	136	276	75 °C	[36]
PAF-25	262	260	75 °C	[36]
SCMP	119.76	345	77 °C, 1 bar	[38]
CalPOF-1	303	477	75 °C, 1 bar	[39]
TPT-BD COF	109	543	75 °C, 1 bar	[40]
TBIM	8.12	943	77 °C, 1 bar	[41]
HBIM	5.27	811	77 °C, 1 bar	[41]

2.1.1.2. Silver-based materials. Silver-based materials have gained a lot of popularity due to their entrapment stability and the ability to withstands high temperatures, humid environments, and high radiation [42,43]. Silver zeolites are the most famous material in this family. Several metals have been tested (Cu, Na, Pb, Ag, Tl, and Cd) for iodine entrapment, and all tests concluded that silver is the best [44]. These materials entrap I_2 by converting it to silver iodide (AgI), which has a low solubility in water (Figure 2.4), making it very stable [42,45,46]. Two main types of zeolites have been investigated for iodine adsorption, which are faujasite X and mordenite [47,48]. The investigations highlighted that Faujasite X demonstrated severe flaws over mordenite that were caused by the low Si/Al ratio leading moisture that strongly reduces its activity [49]. Another study found that the adsorption capacity in these materials was a function of the silver content [43]. Other support materials, like silver titania, have been used [50]. Despite that, these material have several disadvantages, which are: high cost, low capacity, weak recyclability, and low stability when used in nitrogen oxide-rich environment [42,51].

In recent studies, bismuth, the well-established semiconductor, has gained popularity over silver due to its low cost, high adsorption ability, and functionality [52–55]. Several studies has been conducted on its effect on iodine adsorption from a gas stream. In one study by Al-Mamoori [51], mordenite was impregnated by bismuth and tested for iodine adsorption in the gas phase. That study reported a surface area of 412 m^2/g (after Bi impregnation) and iodine uptake capacity of 538 mg/g, which was 48% higher than the reported silver-mordenite [51].

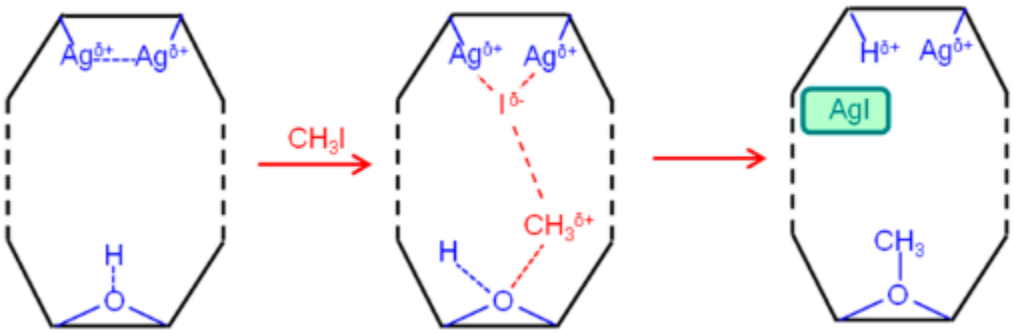

Figure 2.4. The mechanism of reaction between Ag and CH_3I inside the pores of zeolites.

2.1.1.3. Caustic scrubbing. Caustic scrubbing is a process during which a gas stream comes in contact with a caustic solution to remove hazardous gases before releasing them into the atmosphere. In the case of radioactive iodine, NaOH or KOH were the most commonly used caustic solutions[56]. When volatile radioactive iodine comes in contact with a caustic solution (NaOH for example), it reacts with it to produce NaI or $NaIO_3$. The disadvantage of that method is producing an iodine-contaminated solution in large quantities [51,56]. In the review of Riley et al, they listed other scrubbing methods: Mercurex [$Hg(NO_3)_2$] and Iodox. Mercurex has the ability to remove organic and inorganic

iodide; however, mercury is also poisonous, and this technique requires a large amount of it. Iodox uses hyperazeotropic HNO_3 to produce HI_3O_8, which precipitated after evaporating the nitric acid. On the other hand, because of the harsh environment due to using the acid, expensive specialized equipment is needed making Iodox uneconomical [57].

2.1.2. Liquid Phase. Liquid phase radioactive iodine removal is very crucial because it is the pathway to the human body. If the livestock drank contaminated water or the farms were irrigated using that, then their products -like meats and fruits- would be contaminated too.

2.1.2.1. Metal-oxides. Using metal-oxides to remove iodine from the aqueous phase is one of the first approaches scientists investigated. Cations, like Bi^{3+}, Ag^{+}, Pb^{2+}, and Cu^{+}, can react with I^{-} anion and form metal iodide, which is insoluble in water [58–61]. Just like the gas phase, silver was incorporated to remove iodine from aqueous solution. A study by Arixin Bo, where they incorporate silver oxide by grafting it on titania nanolamina, reported a surface area of 143 m^2/g and an adsorption capacity of 3.4 mmol/g after 1 h [62]. Another study impregnated Ag^{+} in MIL-101(Cr)-SO_3H to make MIL-101(Cr)-SO_3Ag using $AgNO_3$ (Figure 2.5). They reported a high adsorption capacity of 244.2 mg/g for the impregnated MIL-101 when compared to 94.1 mg/g for the non-impregnated sample [61].

Similar to the gas phase, many studies in the field of iodine removal from aqueous solutions showed interest in bismuth incorporation. Liu et al prepared a flowlike mesostructured bismuth-oxide ($Bi_2O_{2.33}$) by dissolving bismuth nitrate in ethylene glycol and ethanol, and then heated it in an autoclave for 10 h at 160 ºC before it was filtered,

washed and dried [63]. They reported a surface area of 26.6 m^2/g and an iodine ion removal capacity of 284.90 mg/g [63]. In another study, hierarchically porous bismuth oxide/layered double hydroxide (LDH) was prepared and tested for iodine adsorption. The result from testing LDH fibers before and after Bi_2O_3 impregnation showed an increase in the capacity from 90.1 to 101.9 mg/g with the bismuth-oxide[64]. Han et al synthesized bismuth impregnated graphene-oxide using wet impregnation method [65]. Graphene-oxide is a two-dimentional material synthesized from graphite. They compared it with commercial silver-impregnated zeolites (Ag-Z) and reported an iodine adsorption capacity of 200–230 mg/g, which was higher than Ag-Z [65]. Overall, Bismuth-oxide showed a relatively low capacity due to the low surface area, but when incorporated into a porouse material, it perform like Ag-Z. Table 2.2. summarizes the properties, adsorption capacities and conditions of the materials discussed in this section.

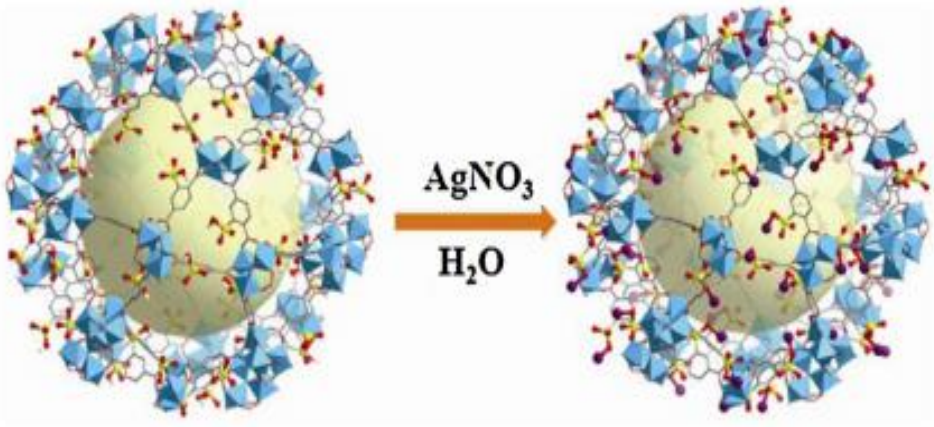

Figure 2.5. MIL-101 3D structure before and after silver impregnation. Atoms' color scheme: red= O, gray= C, yellow= S, blue: Cr, purple: Ag.

Table 2.2. I_2 removal by metal-oxides incorporation.

Material	S_{BET} (m^2/g)	Iodine capture capacity (mg/g)	Conditions	Ref.
Ag_2O–T3NL	135	431	RT	[62]
MIL-101(Cr)-SO_3Ag	861	244.2	30 ºC, 130 rpm	[61]
$Bi_2O_{2.33}$	26.6	284.9	25 ºC, 150 rpm	[63]
Bi_2O_3/LDHs	235	101.9	25 ºC	[64]
Bi-GO	12.7	230	-	[65]

2.1.2.2. MOFs. One of the many versatile applications of MOFs is iodine removal. Despite some MOFs being known for their instability in the presence of water or humidity, UiO-66 MOF is very stable in water and can be synthesized in large scales [66,67]. Wang et al synthesized a high capacity adsorbent for iodine removal using UiO-66 incorporation with pyridine-containing ligands (UiO-66-PYDC) [68]. The high surface area, the water stability, and the scalability of the UiO-66 MOF with pyridine's high affinity for iodine (Figure 2.6) makes this combination a good candidate for iodine removal. The study reported that UiO-66-PYDC had a surface area of 1030 m^2/g and an iodine adsorption capacity of 1250 mg/g [68]. Li et al synthesized a novel MOF/SOF heterostructured framework (MSHC) via self-assembly technique and adding π-conjugated melamine, trimesic acid and Fe^{3+} to build the hybrid network of MOF/SOF. The hybrid material was doped with silver nanocluster to get Ag-MSHC. Ag-MSHC-6, which was shaped like nanorods had the highest affinity toward iodine, recording an adsorption capacity of 771.6 mg/g [69].

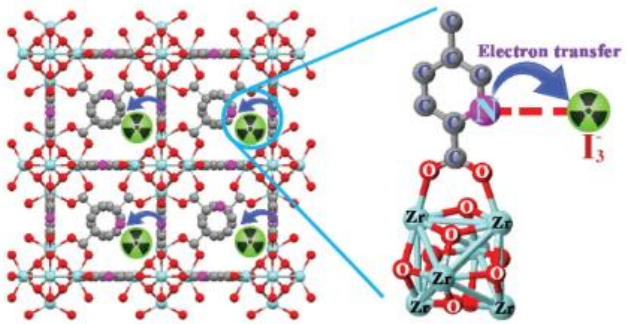

Figure 2.6. A demonstration of the iodine removal mechanism using UiO-66-PYDC. Atoms' color: blue= Zr, gray= C, red= O, green= I_2, purple= N.

2.2. ALUMINA USES IN THE LITERATURE

2.2.1. CO_2 Capture. In the last 20 years, amine functionalized aluminum-oxide has been studied extensively. The promising γ-Al_2O_3 has a large surface area (ranging from 200 to 250 m^2/g), large pore volume (1.2 cm^3/g), and high surface basicity [18,70,71]. Chaikittisilp et al impregnated poly(ethyleneimine) (PEI) on γ-Al_2O_3 surface, using class I method, and they tested its performance before and after steam treatment [18]. They reported a CO_2 capacity of 0.34 mmol/g for the bare γ-Al_2O_3, 1.41 mmol/g for SynA30 (30 wt % PEI@ γ-Al_2O_3). After the steam treatment, the CO_2 capture capacity decreased by 16.3% (from 1.41 to 1.18 mmol/g) [18]. In the same study, bare SBA-15 and 25 wt % PEI@SBA-15 had lower CO_2 capacity before and after steam treatment, despite having a higher surface area of 841 m^2/g for the bare SBA-15 before the steam treatment [18]. The highest CO_2 uptake capacity for a mesoporous alumina (MA) was reported by Chen and Ahn [72]. They synthesized MA using a sol-gel procedure and impregnated PEI onto it. Their investigation revealed a CO_2 uptake capacity of 2.7 mmol/g (0% RH, 75 ^oC, and 1 bar) [72].

In the utilization studies researchers aimed at capturing CO_2 and converting it to syngas via dry ethane reforming (DER). In Al-Mamoori et al's study, γ-Al_2O_3 was used as the support material to incorporate sodium and potassium-based CaO double salts and Ni onto it [71]. The double salts were reported previously for CO_2 capture and the Ni was the catalyst for the reforming reaction [73]. Their investigation showed CO_2 adsorption and desorption capacities for $Ni_{20}@(K{-}Ca)_{50}/(\gamma\text{-}\ Al_2O_3)_{50}$ (DFM-3) of 0.99 and 0.95 mmol/g, respectively, with a 100% ethane conversion [71]. Table 2.3. summarizes the results and the conditions for CO_2 uptake via alumina.

Table 2.3. CO_2 adsorption of amine-functionalized aluminum-oxides.

Material	S_{BET} (m^2/g)	V_P (cm^3/g)	CO_2 capture capacity (mmol/g)	Conditions	Ref.
Bare γ-Al_2O_3	234	1.17	0.34	25 °C, 0.1 bar, 0% RH	[18]
30 wt% PEI@γ-Al_2O_3	111	0.57	1.41	25 °C, 0.1 bar, 0% RH	[18]
Al_2O_3-H_2O-APS-2.85	101	0.48	1.26	25 °C, 0.1 bar, 0% RH	[19]
K_2CO_3@ γ-Al_2O_3	57.7	0.17	2.7	60 °C	[22]
DFM-3	56	0.24	0.99	650 °C, 0.1 bar, 0% RH	[71]
MA	2	0.03	2.7	75 °C, 1 bar, 0% RH	[72]

2.2.2. Iodine Removal via Alumina. There are very few reports about the subject in the literature. One publication from 1994 by Fukasawa and Funabashi used silver-impregnated alumina (AgA) to capture iodine from off-gas streams at nuclear plants[74]. Their investigation revealed that AgA had a surface area of 10 m^2/g and an iodine adsorption capacity of 220 mg/g. Several of the studies reported using silver coated or

silver-impregnated alumina for RI or radionuclides removal [75,76]. New or reliable sources could not be found for iodine removal via alumina. Consequently, a chance to fill the gap in the literature inspired this research to investigate the subject of removing iodine from liquid phase using alumina. The modern alumina techniques and technologies, like using bismuth instead on silver, amine grafting and a combination of both, were employed to fill that gap and solve a serious global problem in the process.

PAPER

I. THE EFFECTS OF AMINE LOADING AND BISMUTH CONTENT ON IODINE IMMOBILIZATION PERFORMANCE OF AMINOSILANE-GRATED Bi/Al_2O_3 ADSORBENTS

Mansour Alsalbokh, Noah Fakeri, Ahmed Al-Mamoori, Ali Rownaghi*, Fateme Rezaei

Deparment of Chemical and Biochemical Engineering, Missouri University of Science and Technology, 1101 N State Street, Rolla, MO 65409, United States

ABSTRACT

In this study, the efficiency of amine-functionalized Bi_x/Al for radioactive iodine removal from water was investigated. Mesoporous alumina was synthesized, impregnated with bismuth using wet impregnation technique, then amine grafted. All the sorbents in this work were characterized with various instruments. N_2 physisorption were used to determine the BET surface area, pore volume, pore width and pore size distribution. FTIR was also used to determine the functional groups before and after grafting. Furthermore, TGA was used to study the thermal stability of the adsorbents. It was found that amine grafting increase the iodine adsorption capacity from 44.7 to 215.7 mg/g. the surface areas of Bi_{15}/Al and Bi_{15}/Al-DMAPS were found to be 219 and 176 m^2/g, respectively. Langmuir and Freundlich isotherm models were plotted to predict the maximum adsorption capacity for Bi_{15}/Al-DMAPS. Langmuir model's calculation revealed a theoretical maximum adsorption capacity of 222.2 mg/g which is very close to the maximum experimental capacity of 215.7 mg/g.

Author Information

Corresponding Authors

Rezaei:*Email: rezaeif@mst.edu; ORCID: 0000-0002-4214-4235

Rownaghi:*Email: rownaghia@mst.edu; ORCID: 0000-0002-5228-5624

1. INTRODUCTION

The U.S. Department of Energy (DOE) has forecasted a nearly 28% increase in demand for electrical energy from 2012 to 2040.[1] This will necessitate a transition to more cost-effective and environmentally-friendly electricity production options such as nuclear energy than other energy sources such as fossil fuels including petroleum and coal. Currently, more than 400 nuclear reactors worldwide produce nearly 11.5% of global electricity.[1] As a major source of electricity generation, the nuclear electricity production is growing steadily to satisfy the worldwide energy demand and is projected to grow between 23 and 100% by 2030.[1,2] Moreover, it does not suffer from the same technological and economic limitations of solar or wind energy. However, nuclear energy is faced with the challenge of the management of radioactive waste produced at each stage of the nuclear fuel cycle, which can limit its growth. Under normal operating conditions, fuel rods used in nuclear power plants need to be reprocessed. This procedure involves the production of complex off-gas mixtures containing radioactive elemental iodine (I-129).[2–4] Such gaseous radioactive waste presents an immediate threat to general population and the environment because of the ease of emission to the atmosphere.

In the past, many aqueous scrubbing concepts including caustic scrubbing (with 1-2 M NaOH) have been explored for iodine capture from off-gas streams. Commonly studied caustic scrubbing solutions for gaseous iodine include those based on the disproportionation reaction that produces NaI, NaIO3, and perhaps NaOI. The result of this process is a liquid residue that can be disposed of as-is or can be further converted to a different form for immobilization. On the other hand, the size and cost of using silver-based solid adsorbent material alone to remove I-129 are relatively large. Recent studies have demonstrated that the combination of a caustic scrubber followed by a solid sorbent polishing bed may reduce the adsorbent usage by ~90%.[2] However, such downstream polishing scrubber has not been well studied.

Development of cheap, non-silver based adsorbents for iodine capture is crucial for wide-spread implementation of adsorbent-based capture technologies in used nuclear fuel (UNF) facilities.[2] Porous solid sorbents have been in the forefront of radioactive contaminant removal due to promising results and their advantages such as high removal efficiency, low maintenance cost, simple equipment design and operation over other techniques.[3] Activated carbons functionalized with amine moieties have been found as potential sorbents for iodine entrapment due to their relatively high capacity, but they have several issues such as decreased capacity and chances of explosion at elevated temperatures.[5] Other traditional sorbents such as silver-impregnated alumina, and silica- and zeolite-based sorbents have been shown to exhibit significant iodine sorption capacity at high temperatures as well. In particular, silver-exchanged mordenite (Ag@MOR) is widely used as a sorbent for capture of iodine because it is mechanically strong, has high efficiency and high loading capacity.[6] In particular, bismuth-based sorbents have

recently received a great deal of attention in iodine capture on the basis of their abundance, low-cost and efficacy.[7,8] Bismuth, when combined with iodine, can form particularly thermodynamically stable compounds such as BiOI and BiI3, as a result of chemisorption-type interactions, which makes bismuth-loaded sorbents promising candidates for long-term iodine disposal.[8–13] In the past, bismuth-doped silica has been extensively studied for gaseous iodine adsorption. For example, a study by Yang et al where thiol-functionalized bismuth-impregnated SBA-15 was synthesized showed an iodine capture capacity of 540 mg/g which was attributed to the affinity between gaseous iodine and Bi2S3 . In our previous investigation, we developed a series of bismuth-doped mordenite adsorbents and evaluated their potential as gaseous iodine capture materials. Our results revealed high uptake capacity and rate over bismuth-samples relevant to the bare mordenite.

Amine-incorporated sorbents have also been considered as suitable candidates for iodine immobilization.[14–16] For example, a recent investigation by Li and co-workers reported a methyl iodide saturation capacity of 71 wt% for tertiary amine- functionalized MIL-101(Cr) which is more than 340% higher than that of Ag@MOR at 150 °C.[5] Further, the material exhibited a relatively fast uptake rate by reaching 48 wt% CH3I uptake within 20 min in comparison to 13 wt% over Ag@MOR within the same time-frame. But generally speaking, reports describing the use of amine-based sorbents for radioactive species have been limited to MOFs. In this work, we report the synthesis of amine-functionalized bismuth sorbents by doping mesoporous γ-alumina support with various amounts of bismuth followed by amine post-functionalization to tether amine moieties on to the surface of Bi/Al. The amine-Bi/Al sorbents thus formed are used to

immobilize iodine from toluene solution. Toluene was chosen because of its high iodine solubility and relatively high boiling point compared to other solvents. Compared to previously reported Bi-Al systems, amine-grafted Bi-Al exhibited outstanding uptakes under both ambient and high temperature (50 ºC) conditions.

2. EXPERIMENTAL SECTION

2.1. MESOPOROUS ALUMINA SYNTHESIS

The mesoporous γ-Al_2O_3 was first synthesized following a procedure reported elsewhere [17] while the bismuth-loaded γ- Al_2O_3 was prepared by the wet impregnation method. In brief, Bismuth (III) sulfide (Bi_2S_3, 99%, Sigma-Aldrich) was first dissolved in nitric acid (HNO_3, Sigma-Aldrich) solution at certain weight ratios. The solution was then diluted with distilled water and stirred for 30 min at room temperature before adding the γ-Al_2O_3 and continue stirring for another 60 min. Next, the solution was filtered under vacuum to obtain the bismuth-loaded γ- Al_2O_3 particles. After that, the filtered particles were dried overnight at 90 ºC. Finally, the particles were calcined at 200 ºC for 4 h with a 1 ºC/min temperature ramp.[9] The bismuth targeted loading was 5, 10, and 15 wt.%. The sorbents prepared with different bismuth loadings were denoted by Bix/ Al_2O_3, where x is weight fraction of bismuth relative to γ- Al_2O_3.

Finally, post-functionalization of Bix/ Al_2O_3 samples was carried out to incorporate amine moieties into their structure. Three aminosilanses were used for grating including primary (3-aminopropyl)-triethoxysilane (APS), secondary (N-methylaminopropyl)trimethoxysilane (MAPS), and tertiary 3-(N,N-

dimethylaminopropyl)trimethoxysilane (DMAPS). In this step, a desired amount of aminosilane was first dissolved in toluene, followed by the addition of degassed Bix/ Al_2O_3 powder and subsequent addition of 2-3 drops of water to initiate grafting. After that, the mixture was placed in a reflux at 80 ºC and let stir for 20 h. After cooling down, the powder was filtered and dried overnight under vacuum at 90 ºC to obtain the final product.[18,19] Synthesis of the adsorbents with similar amine contents enables direct comparison between iodine adsorption characteristics of materials. In this study, the targeted amine loadings were 30, 45 and 60 wt.% for each aminosilane.

2.2. CHARACTERIZATION

The bismuth-impregnated were characterized before and after grafting to study the effect of grafting on various properties. N_2 physisorption analysis was performed at 77 K to estimate the surface area, pore volume, average pore diameter and pore size distribution (PSD) via the Brunauer–Emmmet–Teller (BET) and non-local density functional theory (NLDFT) methods, respectively. Prior to the measurements, the samples were degassed under vacuum at 100 °C for 2 h. Fourier-transform infrared spectroscopy (FTIR) was performed using Thermo Scientific Nicolet iS50 to determine the functional group. All iodine adsorption tests were analyzed using the Hitachi UV-Vis spectrophotometer U-2900. The samples was also assessed using thermal gravimetric analysis (TGA) to investigate their thermal stability. TA Instruments Q500 instrument was used with initial temperature of 25 °C and final one of 900 °C at a rate of 30 °C/min.

2.3. IODINE ADSORPTION TESTS

The test was performed in batches. Each batch had 3 mL of stock iodine solution (0.0025, 0.005, or 0.01 mL/mol) and 30 mg of adsorbent. The test parameters were varied to find the best conditions for the highest adsorption capacity. The parameters were: initial iodine concentration (0.0025, 0.00375, 0.005, 0.0075, 0.008, 0.0085, 0.0095 and 0.01 mol/L), mixing time (2, 4, 8 and 24 h), temperature (25, 50, and 80 ^{o}C), bismuth loading (5, 10, 15, 20 and 30%), amine chain length (primary, secondary and tertiary) and amine loading (30, 45 and 60%). The concentrations of iodine in the samples were determined by the calibration curve which was constructed using the absorbance values of five known concentrations. Furthermore, the iodine solutions were prepared by dissolving iodine in toluene, both were purchased from Sigma-Aldrich. Toluene was chosen because of the high iodine solubility and relatively high boiling point compared to other solvents. The iodine adsorption capacity (q) and removal efficiency ($E_{\%}$) were calculated using the following equations:

$$\text{Adsorption Capacity, q (mg/g)} = \frac{C_i - C_e}{M_S} \times V \quad (1)$$

$$\text{Removal Efficiency, } E_{\%} = \frac{C_i - C_e}{C_i} \times 100 \quad (2)$$

where C_i and C_e are the initial and the residual iodine concentrations in the solution (mg/L), V is the total volume of solution (L), and M_S is the adsorbent amount (g).

2.4. ADSORPTION ISOTHERM MODELS

Langmuir and Freundlich models were used to analyze and represent the iodine adsorption data. Langmuir isotherm model assumes that the surface of the adsorbent is

covered with uniform and homogeneous adsorption sites with a monolayer of adsorbed molecules, whereas Freundlich isotherm model is constructed on the assumptions of a multilayer adsorption with heterogeneous and nonuniform adsorption sites.[20] The Langmuir and Freundlich isotherm models can be mathematically expressed in the linear form by Equation 3 and Equation 4, respectively:

$$\frac{C_e}{Q_e} = \frac{1}{Q_{\max} K_L} + \frac{C_e}{Q_{\max}} \quad (3)$$

$$Log\left(Q_e\right) = Log\left(K_f\right) + \frac{Log\left(C_e\right)}{n} \quad (4)$$

where Q_e is the adsorption amount (mg/g), Q_{max} is the maximum adsorption capacity (mg/g), K_L is Langmuir constant, K_f is Freundlich constant and n is Freundlich exponent.

3. RESULTS

3.1. CHARACTERIZATION

The obtained N_2 physisorption isotherms are presented in Figure 1 along with the corresponding pore size distribution (PSD) profiles. Consistent with the bare alumina, the Bi_x/Al_2O_3 and their corresponding amine-grafted analogues all exhibited type IV isotherm with an H1 hysteresis loop which is indicative of their mesoporous structure. Notably, by increasing bismuth loading the N_2 uptake was reduced over the Bi_x/Al_2O_3 adsorbents. Moreover, it can be observed that the samples grafted with DMAPS gave rise to higher N_2 uptake than APS- and MAPS-grafted materials. The PSD curves in Figure 1b displayed a

shift in pore size to a smaller values after amine incorporation, but overall, the PSD for the grafted materials were uniform in the range of 9-12 nm.

The physical characteristics of the bare alumina support, Bix/Al2O3 and amine-functionalized Bix/Al2O3adsorbents used in this study, along with the amine loadings of the materials are reported in Table 1. As expected, the surface area and pore volume decreased upon both bismuth doping and amine grafting. A decreasing trend in surface area and pore volume was observed with increasing bismuth loading. For example, the surface area decreased from 251 m^2/g from bare γ- Al_2O_3 to 256, 220, and 219 m^2/g for Bi_5/Al, Bi_{10}/Al, and Bi_{15}/Al respectively. It was also noted that among the grafted samples, adsorbents that were grafted with the same amount of DMAPS possessed higher surface area than those grafted with APS and MAPS.

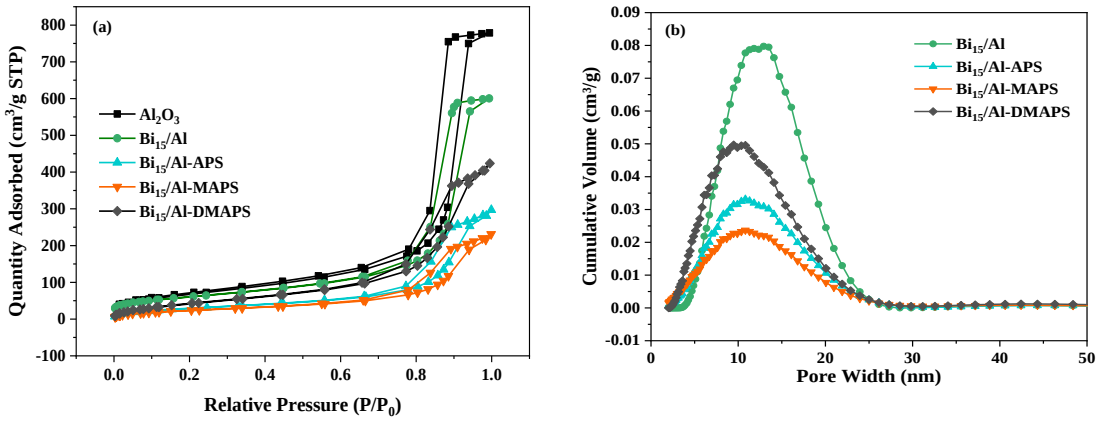

Figure 1. N_2 physisorption isotherms (a) and pore size distribution profiles (b) for Bi_x/Al_2O_3 samples before and after grafting.

Table 1. Textural properties of Bi_x/Al_2O_3 before and after amine grafting with 30 wt% aminosilane.

Adsorbent	**S_{BET} (m^2/g)**	**V_p (cm^3/g)**	**d_p (nm)**
Bare Al_2O_3	251	1.177	14
Bi_5/Al	256	0.870	11
Bi_{10}/Al	220	0.971	13
Bi_{15}/Al	219	0.926	13
Bi_{15}/Al-APS	113	0.413	11
Bi_{15}/Al-MAPS	92	0.320	10
Bi_{15}/Al-DMAPS	176	0.599	10

To further confirm the grafting of aminosilanes into the Bi-doped alumina, the FTIR analysis was performed on the samples across wavelength range of 4000-400 cm^{-1} and the corresponding spectra are presented in Figure 2. Across the three sets of Bi_x/Al materials, the presence of similar characteristics peaks is evident in all the spectra shown in this figure. The vibrational band at 3450 and 1640 cm^{-1} can be attributed to –OH stretching and H–O–H bending, respectively, whereas the peaks at 515, 720 and 1041 cm^{-1} are ascribed to the Al–O (AlO_6 octahedron), Al–O (AlO_4 tetrahedron) stretching, and Al–OH bending, respectively.[21–23] Furthermore, the bands in 3050, 2930 and the 1600-1450 cm^{-1} range are all related to the C–N stretching, whereas the peaks in the 1400-1300 cm^{-1} range correspond to the N–O stretching [24–26], indicating the presence of amine moieties in the grafted samples. The presence of a peak at 1470 cm^{-1} in the spectra of grafted samples is associated with carbonate species which was formed by the attraction between the basic O^{2-} active sites and CO_2 in the air [27]. The spectra for the iodine-loaded samples are also displayed in Figure 2. It was noticed that there were not any structural changes to the adsorbents after the iodine adsorption tests. The iodine-loaded samples also

showed a sizable increase at 3450, 1640, 1470 and 1041 cm^{-1} which could indicate that iodine was adsorbed on these sites which corresponds to –OH and C—N stretching via the chemisorption phenomenon.

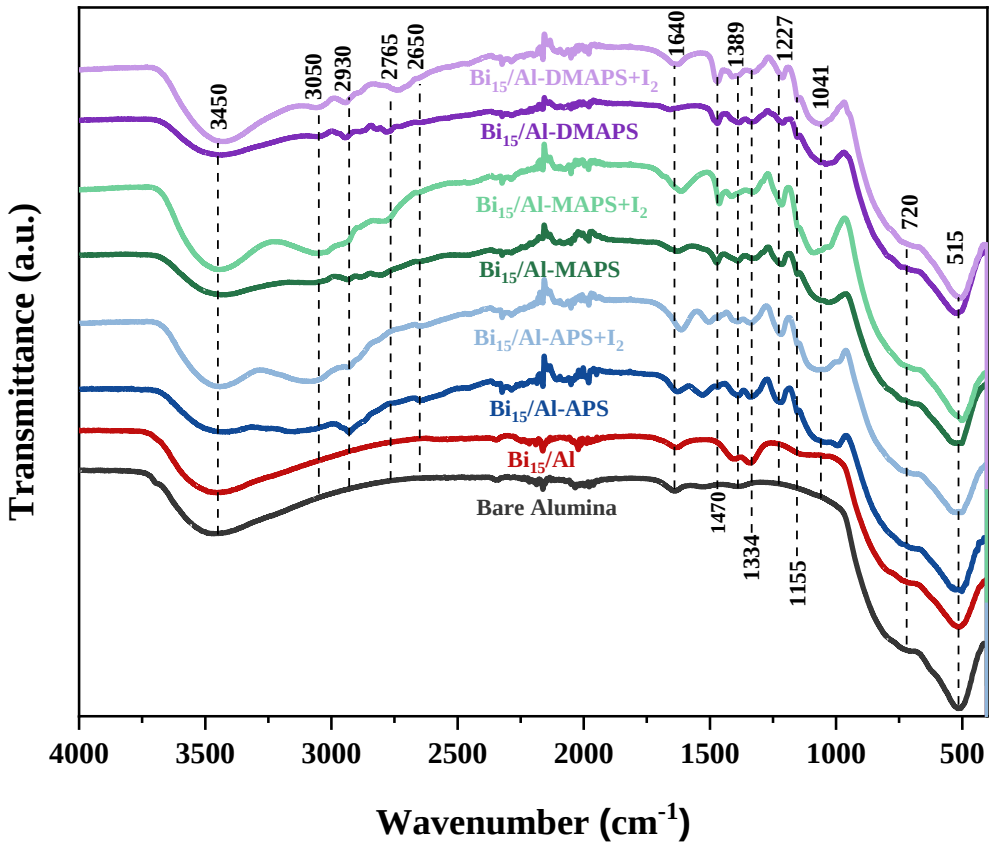

Figure 2. FTIR spectra of for bare alumina, Bi_x/Al_2O_3 and amine-grafted Bi_x/Al_2O_3.

3.2. THE ADSORPTION OF IODINE Bi_x/Al

The effect of bismuth loading on iodine removal performance of the adsorbents was investigated under identical experimental conditions, (i.e., at 80 °C temperature, with 0.0025 mol/L iodine concentration, and at 24 h). 80 °C was chosen based on literature review. The UV-Vis spectra of iodine in toluene after the adsorption test with Bi_x/Al_2O_3

and the stock solution (solution without adsorbent) are shown in Figure 3a, where iodine in toluene exhibits a peak at 498±3 nm. The peak's intensities or absorbance then were translated in term of removal efficiency (Equation 2) as a function of bismuth loading and presented in Figure 3b. An increasing trend in iodine removal capacity was observed with bismuth content from 5 to 15 wt%. To demonstrate if there is an optimal content for bismuth, two additional samples were prepared with 20 and 30 wt% Bi and tested under the same conditions. As can be seen further increase in the amount of doped bismuth did not give rise to improved removal efficiency and beyond 15 wt%, an opposite trend was noted which likely due to reduced surface area of the alumina in these samples. Moreover, while the Bi_5@Al and Bi_{10}@Al exhibited 20 and 50% removal efficiency, a maximum efficiency of 70% was estimated from the UV-Vis profiles for Bi_{10}@Al. On the contrary, the removal efficiency was reduced to below 20% for Bi_{20}/Al and Bi_{30}/Al samples. This could be attributed to pore blockage that might prevent iodine from getting in the pores of the mesoporous alumina.

In Figure 4, a comparison between iodine adsorption capacities of Bi_x/Al samples at 80 ºC is illustrated. As expected, the adsorption capacity improved from 14.2 mg/g for Bi_5/Al to 30.5 and 44.7 mg/g for Bi_{10}/Al and Bi_{15}/Al, respectively. A 214% increase in iodine immobilization capacity by increasing bismuth content from 5 wt% to 15 wt% indicating the promotional effect of bismuth on immobilization of iodine from aqueous solutions. On the basis of these screening results and in light of high iodine adsorption capacity and removal efficiency, Bi_{15}/Al was chosen for further analysis to find the maximum iodine capacity at the optimal immobilization conditions.

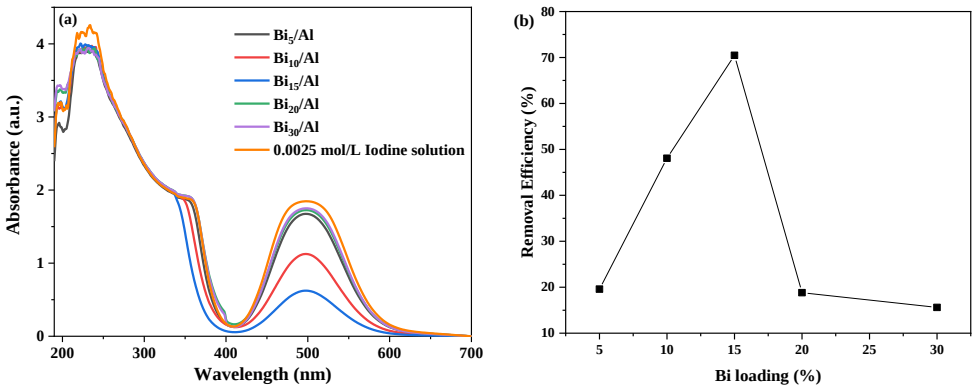

Figure 3. (a) UV-Vis spectra of Bi_x/Al samples and (b) the corresponding iodine removal efficiency as a function of Bi loading.

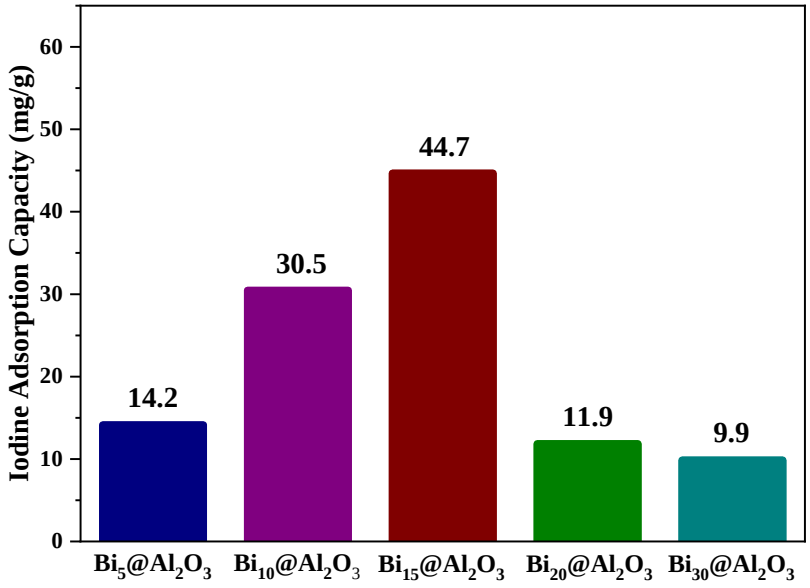

Figure 4. Iodine adsorption capacity of Bi_x/Al samples with varying bismuth loadings at 80 °C.

The effect of contact time on iodine adsorption performance of the adsorbents was investigated by analyzing the iodine solutions-loaded materials with UV-Vis at various times within 1-24 h time frame. As can be seen in Figure 5, iodine adsorption over Bi_{15}/Al

increased with time until 8 h, however, as time progressed, removal efficiency reduced and longer times resulted in deteriorated capacity. This could be due to leaching of adsorbed iodine from the adsorbent which resulted in an 11% lower removal efficiency after 24 h compared to that after 8 h. On the other hand, the relatively sharp increase in iodine uptake in the beginning of adsorption is due to higher concentration gradient between the solution and the adsorbent pores. Here, the observed trend suggests a weak adsorption interaction between the adsorption sites on Bi_{15}/Al surface and the iodine species, leading to iodine desorption from the adsorbent over time.

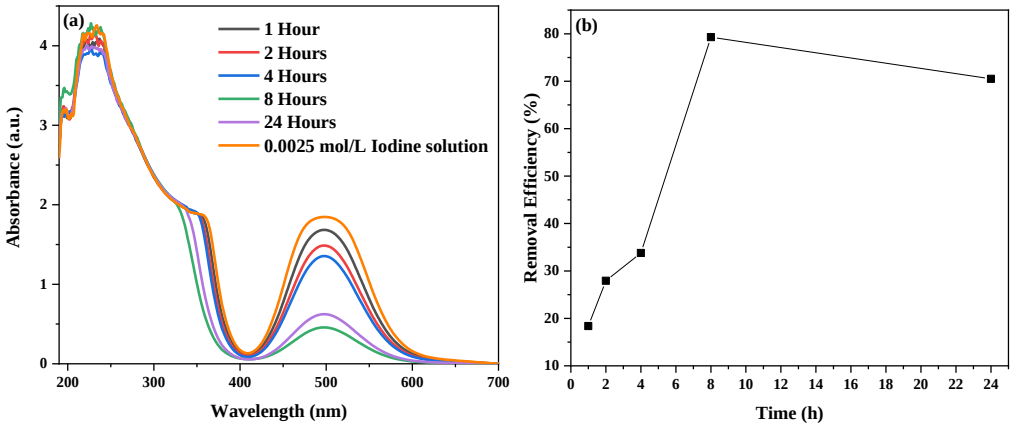

Figure 5. (a) UV-Vis spectra of Bi_{15}/Al at 80 °C and (b) the corresponding iodine removal efficiency as a function of time.

Although the screening tests were conducted at elevated temperatures (80 ºC), we also examined the iodine removal efficiency of the selected adsorbent (Bi_{15}/Al) after 24 h at 25 and 50 °C while keeping the iodine concentration fixed at 0.0025 mol/L. It is apparent from Figure 6 that upon increasing temperature, iodine adsorption increases up to 50 ºC, followed by reduced capture at higher temperatures, as a result of thermodynamic effects,

as expected. Specifically, the results indicated that for the system investigated here, 50 °C is an optimal temperature for iodine adsorption which results in 94.7% removal efficiency, relevant to 40.2% at 25 ºC and 61.5% at 80 ºC.

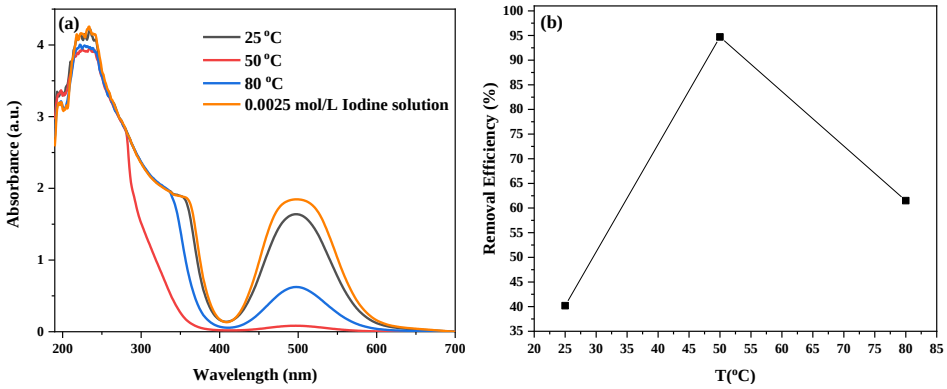

Figure 6. (a) UV-Vis spectra of Bi_{15}/Al at various temperatures, and (b) the corresponding iodine removal efficiency as a function of adsorption temperature.

3.3. IODINE ADSORPTION ON AMINE-GRAFTED Bi_{15}/Al_2O_3

To demonstrate the dependency of iodine adsorption on amine type, we performed the same set of tests on amine-grafted Bi_{15}/Al namely, Bi_{15}/Al-APS, Bi_{15}/Al-MAPS, and Bi_{15}/Al-DMPAS. As the removal efficiency of Bi_{15}/Al was highest at 50 °C, we conducted the measurements on grafted adsorbents at this optimal temperature. The iodine capacities of the grafted samples are reported in Figure 7. It was observed that whereas the primary amine (APS) only gave rise to marginal enhancement in iodine removal from the solution, grafting with the tertiary amine (DMAPS) produced the highest improvement exhibiting an adsorption capacity of 215.7 mg/g which was 258.9% higher than that of bare Bi_{15}/Al. This could be attributed to the chemisorption phenomenon where iodine reacts with the

amine group from the aminosilane and entraps iodine within the mesoporous structure of the alumina.

In the next step, we investigated how adsorption behavior of our best performing material (Bi15/Al-DMPAS) changes over time, in a similar way to its un-grafted analogue (Bi15/Al). Surprisingly, iodine adsorption kept increasing with time over this material, as evident from Figure 7. It was also noticed that amine efficiency dramatically improved and tha capacity reached 215.7 mg/g, relative to 60.1 mg/g for bare Bi_{15}/Al, implying that by incorporation of amine moieties into the Bi/Al_2O_3, the iodine leaching over time can be inhibited. We hypothesize that the stronger chemical interactions between the amine-grafted adsorbents and the iodine species (i.e., chemisorption), leads to a better retainment of the adsorbed iodine within the pores of Bi_{15}/Al-DMPAS. This is an important finding since the iodine-loaded samples need to demonstrate minimal iodine leaching for safe disposal into geological reservoirs. It should also be noted here that although the iodine-loaded materials are not directly disposed of and should be processed into a durable waste form prior to permanent storage.

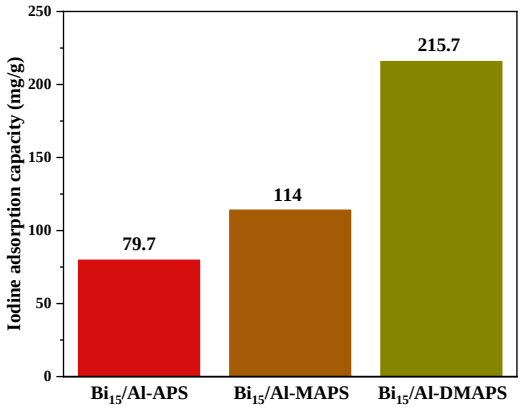

Figure 7. Iodine adsorption capacities after grafting with APS, MAPS and DMAPS.

To further demonstrate how amine content impacts the iodine removal efficiency of Bi15/Al-DMPAS, Bi15/Al was grafted with 45 and 60 wt% DMPAS and the amine-functionalized adsorbents were then tested alongside our reference adsorbent (Bi15/Al-DMPAS) at 50 ºC using a stock solution of 0.01 mol/L iodine. DMAPS was chosen for this test due to its superior adsorption capacity compared to APS and MAPS, as demonstrated before. Our results indicated that increasing amine loading has a positive effect on iodine immobilization from toluene solution. In particular, the capture capacity was enhanced from 215.7 mg/g for 30 wt% DMAPS to 241.1 and 251.7 mg/g for 45 and 60 wt% DMAPS, respectively which were about 11 and 16% improvement. Compared to other bismuth-oxides and bismuth-doped materials from the literature (Table 2.), Bi_{15}/Al-DMPAS is on par or better in term of removal capacity. It should be noted here that we chose not to increase amine loading beyond 60 wt% as higher loadings usually have an opposite effect and result in a dramatic decrease in surface area and pore volume of the support, which will in turn reduce adsorption capacity.

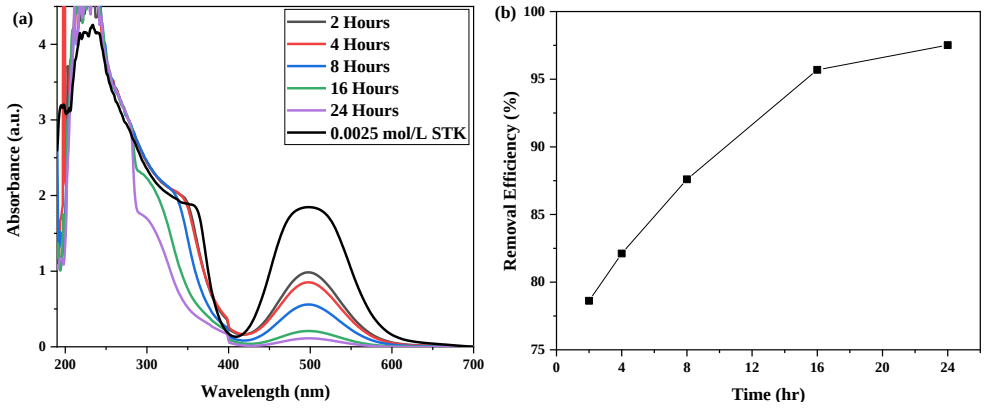

Figure 8. (a) UV-Vis spectra of Bi_{15}/Al-DMAPS at 50 °C, and (b) the corresponding removal efficiency as a function of time.

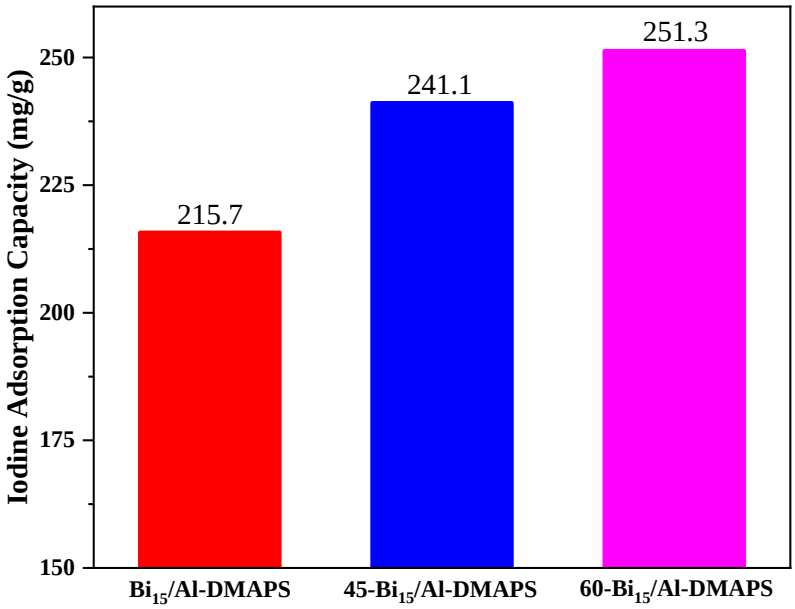

Figure 9. Iodine adsorption capacity for Bi_{15}/Al-DMAPS with varying amine loading at 50 °C.

Table 2. A comparison of other adsorbents used for iodine removal from a liquid phase.

Material	**Capacity (mg/g)**	**Reference**
60 Bi_{15}/Al-DMPAS	251.3	This work
$Bi_2O_{2.33}$	284.9	[28]
Bi_2O_3/LDH	101.9	[29]
Bi-GO	230	[12]

Langmuir and Freundlich adsorption models were used to analyze the data obtained from the experimental work. The iodine capture data for Bi15/Al-DMAPS with 30 wt% amine loading from varying the initial iodine concentration test were used with the linear forms of the two models to find the theoretical maximum for iodine adsorption capacity (50 oC, 15 wt% Bi loading, DMAPS). For Langmuir model, Ce/qe was plotted as a function of Ce (Figure 9a) and the best fit was used to get the slope and intercept. The slope was

then used to calculate qmax which was 222.2 mg/g for this sample. With this calculated qmax (222.2 mg/g) which almost matched the experimental capacity (215.7 mg/g) and with an R^2 value of 0.994, it was concluded that Langmuir model is a suitable model to accurately describe the adsorption behavior. For Freundlich model on the other hand (Figure 9b), qe versus Ce was plotted in logarithmic form and the best fit was used to find the slope and intercept. Notably and unlike Langmuir model, the Freundlich model showed more variance (R^2 = 0.82), indicating that this model is not the best model to describe the behavior of iodine adsorption on Bi_{15}/Al-DMAPS. The Freundlich constant, *kf*, and exponent, *n*, were calculated, as listed in Table 3 along with the Langmuir parameters.

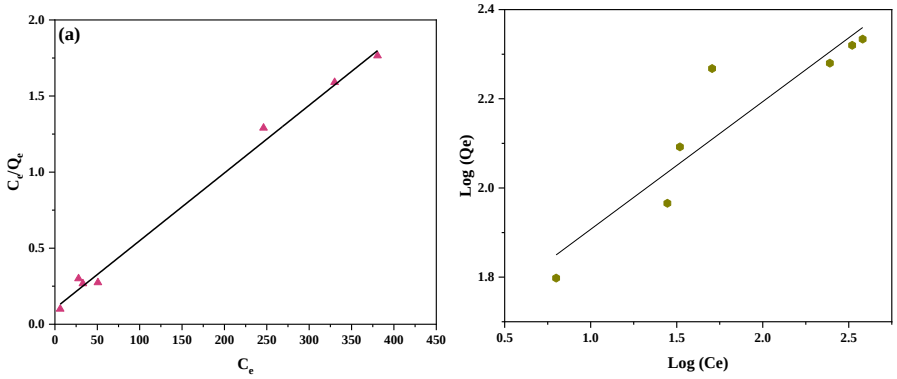

Figure 10. (a) Langmuir and (b) Freundlich models for iodine adsorption on Bi_{15}/Al-DMAPS with 60 wt% amine loading.

Table 3. The parameters for Langmuir and Freundlich adsorption isotherm for iodine adsorption.

	Langmuir			Freundlich		
$q_{max\ Exp}$ (mg/g)*	q_{max} (mg/g)	k_L (L/mg)	R^2	k_f	*n*	R^2
215.7	222.2	0.043	0.994	41.8023	3.4953	0.8595

*Maximum experimental capacity.

4. CONCLUSIONS

In this work, we investigated the adsorption performance of bismuth-doped mesoporous alumina along with its amine-functionalized analogues for the removal of elemental iodine from an aqueous solution of toluene. Bismuth loading of 15 wt% was found to be an optimal loading on the basis of its highest iodine removal efficiency. Investigation of adsorption temperature revealed that iodine removal efficiency is the highest at 50 ºC, reaching 60.1 mg/g for Bi_{15}/Al. However, this sample demonstrated some degree of iodine leaching after 8 h exposure time, which resulted in 11% loss in adsorption capacity after 24 h. Moreover, the iodine capture tests on amine-grafted adsorbents revealed DMAPS to be the most efficient aminosilane to enhance the iodine capture capacity of Bi_{15}/Al. Our investigation of amine loading impact on removal efficiency showed that by doubling DMAPS content from 30 to 60 wt%, the adsorption capacity increases by 16% reaching the highest value of 251.7 mg/g at 50 ºC for the samples investigated here. More importantly, it was found that by functionalizing Bi/Al_2O_3 with aminosilanes, the issue of iodine retainment over time can be adequately addressed. Overall, the findings of this work highlight the potential utility of bismuth-alumina adsorbents functionalized with aminosilanes as adsorbent materials for immobilization of iodine from iodine-containing aqueous solutions.

ACKNOWLEDGEMENTS

Mansour Alsalbokh would like to acknowledge Saudi Arabian Cultural Mission to the US (SACM) for their financial support.

REFERENCES

[1] W.N. Association, World Energy Needs and Nuclear Power, Http://Www. World-Nuclear.Org/Information-Library/Current-and-Future-Generation/Worldenergy-Needs-and-Nuclear-Power.Aspx. (2017).

[2] B.J. Riley, J.D. Vienna, D.M. Strachan, J.S. McCloy, J.L. Jerden, Materials and processes for the effective capture and immobilization of radioiodine: A review, J. Nucl. Mater. 470 (2016) 307–326. https://doi.org/10.1016/j.jnucmat.2015.11.038.

[3] S.U. Nandanwar, K. Coldsnow, V. Utgikar, P. Sabharwall, D. Eric Aston, Capture of harmful radioactive contaminants from off-gas stream using porous solid sorbents for clean environment – A review, Chem. Eng. J. 306 (2016) 369–381. https://doi.org/10.1016/j.cej.2016.07.073.

[4] S.H. Bruffey, R.T. Jubin, J.A. Jordan, Capture of Elemental and Organic Iodine from Dilute Gas Streams by Silver-exchanged Mordenite, Procedia Chem. 21 (2016) 293–299. https://doi.org/10.1016/j.proche.2016.10.041.

[5] B. Li, X. Dong, H. Wang, D. Ma, K. Tan, S. Jensen, B.J. Deibert, J. Butler, J. Cure, Z. Shi, T. Thonhauser, Y.J. Chabal, Y. Han, J. Li, Capture of organic iodides from nuclear waste by metal-organic framework-based molecular traps, Nat. Commun. 8 (2017). https://doi.org/10.1038/s41467-017-00526-3.

[6] K.W. Chapman, P.J. Chupas, T.M. Nenoff, Radioactive iodine capture in silver-containing mordenites through nanoscale silver iodide formation, J. Am. Chem. Soc. 132 (2010) 8897–8899. https://doi.org/10.1021/ja103110y.

[7] J.H. Yang, J.M. Shin, J.J. Park, G. Il Park, M.S. Yim, Novel synthesis of bismuth-based adsorbents for the removal of 129I in off-gas, J. Nucl. Mater. 457 (2015) 1–8. https://doi.org/10.1016/j.jnucmat.2014.09.057.

[8] J.H. Yang, Y.J. Cho, J.M. Shin, M.S. Yim, Bismuth-embedded SBA-15 mesoporous silica for radioactive iodine capture and stable storage, J. Nucl. Mater. 465 (2015) 556–564. https://doi.org/10.1016/j.jnucmat.2015.06.043.

[9] A. Al-Mamoori, M. Alsalbokh, S. Lawson, A.A. Rownaghi, F. Rezaei, Development of bismuth-mordenite adsorbents for iodine capture from off-gas streams, Chem. Eng. J. (2019). https://doi.org/10.1016/j.cej.2019.123583.

[10] J.L. Krumhansl, T.M. Nenoff, Hydrotalcite-like layered bismuth-iodine-oxides as waste forms, Appl. Geochemistry. 26 (2011) 57–64. https://doi.org/10.1016/j.apgeochem.2010.11.003.

[11] L. Zhang, A.A.S. Gonçalves, B. Jiang, M. Jaroniec, Capture of Iodide by Bismuth Vanadate and Bismuth Oxide: An Insight into the Process and its Aftermath, ChemSusChem. 11 (2018) 1486–1493. https://doi.org/10.1002/cssc.201800327.

[12] S. Han, W. Um, W.S. Kim, Development of bismuth-functionalized graphene oxide to remove radioactive iodine, Dalt. Trans. 48 (2019) 478–485. https://doi.org/10.1039/C8DT03745K.

[13] J.H. Yang, H.S. Park, D.H. Ahn, M.S. Yim, Glass composite waste forms for iodine confined in bismuth-embedded SBA-15, J. Nucl. Mater. 480 (2016) 150–158. https://doi.org/10.1016/j.jnucmat.2016.08.001.

[14] A. Ahmadalinezhad, A. Sayari, Oxidative degradation of silica-supported polyethylenimine for CO2 adsorption: insights into the nature of deactivated species., Phys. Chem. Chem. Phys. 16 (2013) 1529–1535. https://doi.org/10.1039/c3cp53928h.

[15] A. Sayari, Y. Belmabkhout, E. Da'na, CO2 deactivation of supported amines: does the nature of amine matter?, Langmuir. 28 (2012) 4241–7. https://doi.org/10.1021/la204667v.

[16] P. Bollini, S. Choi, J.H. Drese, C.W. Jones, Oxidative Degradation of Aminosilica Adsorbents Relevant to Postcombustion CO2 Capture, Energy & Fuels. 25 (2011) 2416–2425.

[17] A. Al-Mamoori, A.A. Rownaghi, F. Rezaei, Combined Capture and Utilization of CO2 for Syngas Production over Dual-Function Materials, ACS Sustain. Chem.Eng. 6 (2018) 13551–13561. https://doi.org/10.1021/acssuschemeng.8b03769.

[18] S. Lawson, C. Griffin, K. Rapp, A.A. Rownaghi, F. Rezaei, Amine-Functionalized MIL-101 Monoliths for CO 2 Removal from Enclosed Environments, Energy and Fuels. 33 (2019) 2399–2407. https://doi.org/10.1021/acs.energyfuels.8b04508.

[19] T. Gelles, S. Lawson, A.A. Rownaghi, F. Rezaei, Recent advances in development of amine functionalized adsorbents for CO2 capture, Springer US, 2020. https://doi.org/10.1007/s10450-019-00151-0.

[20] R. Kecili, C. Mustansar Hussain, Chapter 4 - Mechanism of Adsorption on Nanomaterials, in: 2018: pp. 89–115.

[21] X. Du, Y. Wang, X. Su, J. Li, Influences of pH value on the microstructure and phase transformation of aluminum hydroxide, Powder Technol. 192 (2009) 40–46. https://doi.org/10.1016/j.powtec.2008.11.008.

[22] J. Gangwar, B.K. Gupta, S.K. Tripathi, A.K. Srivastava, Phase dependent thermal and spectroscopic responses of Al2O3 nanostructures with different morphogenesis, Nanoscale. 7 (2015) 13313–13344. https://doi.org/10.1039/c5nr02369f.

[23] L. Shen, C. Hu, Y. Sakka, Q. Huang, Study of phase transformation behaviour of alumina through precipitation method, J. Phys. D. Appl. Phys. 45 (2012). https://doi.org/10.1088/0022-3727/45/21/215302.

[24] F. Rezaei, C.W. Jones, Stability of supported amine adsorbents to SO2 and NO x in postcombustion CO2 capture. 1. single-component adsorption, Ind. Eng. Chem. Res. 52 (2013) 12192–12201. https://doi.org/10.1021/ie4019116.

[25] J. Coates, Encyclopedia of Analytical Chemistry -IInterpretation of Infrared Spectra, A Practical Approach, Encycl. Anal. Chem. (2004) 1–23. http://www3.uma.pt/jrodrigues/disciplinas/QINO-II/Teorica/IR.pdf.

[26] F. Rezaei, M.A. Sakwa-Novak, S. Bali, D.M. Duncanson, C.W. Jones, Shaping amine-based solid CO2 adsorbents: Effects of pelletization pressure on the physical and chemical properties, Microporous Mesoporous Mater. 204 (2015) 34–42. https://doi.org/10.1016/j.micromeso.2014.10.047.

[27] M.E. Potter, K.M. Cho, J.J. Lee, C.W. Jones, Role of Alumina Basicity in CO2 Uptake in 3-Aminopropylsilyl-Grafted Alumina Adsorbents, ChemSusChem. 10 (2017) 2192–2201. https://doi.org/10.1002/cssc.201700115.

[28] S. Liu, S. Kang, H. Wang, G. Wang, H. Zhao, W. Cai, Nanosheets-built flowerlike micro/nanostructured Bi2O2.33 and its highly efficient iodine removal performances, Chem. Eng. J. 289 (2016) 219–230. https://doi.org/10.1016/j.cej.2015.12.101.

[29] T. Zhang, X. Yue, L. Gao, F. Qiu, J. Xu, J. Rong, J. Pan, Hierarchically porous bismuth oxide/layered double hydroxide composites: Preparation, characterization and iodine adsorption, J. Clean. Prod. 144 (2017) 220–227. https://doi.org/10.1016/j.jclepro.2017.01.030.

II. ADSORPTION OF IODINE FROM AQUEOUS SOLUTION BY AMINOSILANE-GRAFTED MESOPOROUS ALUMINA: EFFECTS OF AMINE TYPE AND CONTENT

Mansour Alsalbokh, Noah Fakeri, Shane Lawson, Ali Rownaghi*, Fateme Rezaei*

Deparment of Chemical and Biochemical Engineering, Missouri University of Science and Technology, 1101 N State Street, Rolla, MO 65409, United States

ABSTRACT

In this study, we present a detailed investigation of the performance of a series of bismuth-loaded alumina adsorbents (Bi/Al) grafted with three different aminosilanes including 3-Aminopropyl-triethoxysilane (APS), N-methylaminopropyl-trimethoxysilane (MAPS), and 3-N,N-dimethylaminopropyl-trimethoxysilane (DMAPS), in the removal of iodine from aqueous solutions. Specifically, we studied the effects of bismuth loading, amine type and content, as well as iodine concentration and capture temperature to determine the best performing material and removal condition for iodine immobilization from caustic scrubber solutions. Our results indicated that amine grafting can enhance the iodine removal performance of Bi-Al, with DMAPS giving rise to highest capacity. It was also found that iodine capture over amine-grafted Bi/Al changes dramatically with amine content. Among the materials investigated, Bi_5/Al-DMAPS with an amine content of 60 wt% exhibited the highest iodine capture capacity of 215.7 mg/g at 50 ºC. Moreover, amine grafting improved the retention of adsorbed iodine species within the adsorbent over time with no degree of leaching after 24 h, unlike Bi/Al_2O_3 analogue resulted in the iodine removal efficiency of the adsorbents was found to be a strong function of temperature.

Keywords: Iodine capture, Adsorption, Aminosilane, Alumina, Removal Efficiency

Author Information

Corresponding Authors

Rezaei:*Email: rezaeif@mst.edu; ORCID: 0000-0002-4214-4235

Rownaghi:*Email: rownaghia@mst.edu; ORCID: 0000-0002-5228-5624

1. INTRODUCTION

Radioactive materials (RMs) have gained popularity in the last decades and their applications are being used across several fields. RMs have been used for diagnosing and treating cancers, producing energy, tracers for industrial applications, etc [1–3]. For power generation, nuclear power generation is more favorable than the traditional combustion methods because it produce less waste. On the other hand, nuclear waste are substantially more dangerous than the waste produced by combustion [2]. A 2011 study revealed that 14% of the world's power generation was produced by nuclear power plants (NPPs) [4]. Radioiodine or radioactive iodine (RI) is one of the nuclear wastes produced by the fission reaction of uranium [5]. RI is present in two forms: ^{131}I which has a half-life of 8 days and ^{129}I which has a half-life of 15.7 million years [6,7]. The fact that RI could exist as a gas or in water makes it very alarming. RI can contaminate the soil and irrigation water which will, as a result, contaminate the farms and dairy products [5].

Since metal-based adsorbents showed promise in removing RI from the gas phase [8–13], researchers developed them for the liquid phase. Cations, like Bi^{3+}, Ag^{+}, Pb^{2+}, and Cu^{+}, can react with I^{-} anion and form metal iodide which is insoluble in water[14–17]. A

study by Arixin Bo, where they incorporate silver oxide by grafting it on titania nanolamina, reported a surface area of 143 m^2/g and adsorption capacity of 3.4 mmol/g after 1 h [18]. Another study impregnated Ag^+ in MIL-101(Cr)-SO3H to make MIL-101(Cr)-SO3Ag using AgNO3. They reported a high adsorption capacity of 244.2 mg/g for the impregnated MIL-101 compared to 94.1 mg/g for the non-impregnated one [17]. Like silver, bismuth and bismuth-oxide, the well-established semiconductor, have their share of attention due to their low cost, adsorption ability, nontoxicity, and functionality [19–23]. Liu et al prepared a flowlike mesostructured bismuth-oxide ($Bi_2O_{2.33}$) by dissolving bismuth nitrate in ethylene glycol and ethanol, and then heated in an autoclave for 10 h at 160 ^oC before it was filtered, washed and dried. They reported a surface area of 26.6 m^2/g and an iodine ion removal capacity of 284.90 mg/g [24]. In another study, hierarchically porous bismuth oxide/layered double hydroxide (LDH) was prepared and tested for iodine adsorption. The result from testing LDH fibers before and after Bi_2O_3 impregnation showed an increase in the capacity from 90.1 to 101.2 mg/g with the bismuth-oxide [25].

2. EXPERIMENTAL PROCEDURE

2.1. ADSORBENT SYNTHESIS

γ-Al_2O_3 was synthesized according to a procedure reported elsewhere [26]. Briefly, 13.75 g of pseudoboehmite Catapal B (Sasol) was peptized in a mixture of nitric acid (1.27 g) and distilled water (200 mL). The mixture was sonicated at room temperature for 90 min and then stirred for 17 h at 60 °C. Next, the suspension was left to cool down to room

temperature. Then, Pluronic P123 EO20- PO70-EO20 triblock copolymer (Sigma-Aldrich, 15.3 g) dissolved in (200 mL) ethanol was added gradually to the peptized alumina while stirred at room temperature. The mixture was kept under stirring for 24 h at room temperature. After that, the suspension was heated to 60 ^{o}C for 60 h in an open beaker in the fume hood to remove the solvent. The remaining material was dried at 75 °C for 24 h and calcined in two steps: first at 150 °C for 1 h to remove the remaining water and ethanol with a ramp of 1 °C/min and the second at 700 °C for 4 h.

2.2. AMINE GRAFTING

Three amines with three different chain lengths were used for grating. (3-Aminopropyl)-triethoxysilane (APS), (N-methylaminopropyl)trimethoxysilane (MAPS), and 3-(N,N-dimethylaminopropyl)trimeth-oxysilane (DMAPS). First, amine was dissolved in toluene with respect to the required amine loading. Then, γ-Al_2O_3 powder was added before adding 2-3 drops of water to initiate the grafting. After that, the mixture was placed in a reflux at 80 ^{o}C for 20 h. After cooling down, the powder was filtered and dried overnight under vacuum at 90 ^{o}C. [27,28]

2.3. ADSORBENT CHARACTERIZATION

The characterization study on the alumina adsorbents were done via the following instruments. N_2 physisorption isotherms analysis at 77 K was performed to estimate the surface area and the pore volume via the Brunauer–Emmmet–Teller (BET) and non-local density functional theory (NLDFT) methods, respectively. Prior to the measurements, the samples were degassed under vacuum at 100 °C for 3 h. All iodine adsorption tests were

analyzed using the Hitachi UV-Vis spectrophotometer U-2900. Fourier-transform infrared spectroscopy (FTIR) was performed using Thermo Scientific Nicolet iS50 to determine the functional group.

2.4. IODINE REMOVAL TESTS

The test was performed in batches. Each batch had 3 mL of stock iodine solution (0.0025, 0.005, or 0.01 mL/mol) and 30 mg of adsorbent. The test parameters were varied to find the best conditions for the highest adsorption capacity. The parameters were: initial iodine concentration (0.0025, 0.004, 0.005, 0.0065, 0.0085 and 0.01 mol/L), temperature (25, 50, and 80 ^{o}C), amine's chain length (primary, secondary and tertiary), and amine loading (30, 40 and 50%). The concentrations of iodine in the samples were determined by the calibration curve which was constructed using the peak's height of five known concentrations. Furthermore, the iodine solutions were prepared by dissolving iodine in toluene (both were purchased from Sigma-Aldrich). Toluene was chosen because of the high iodine solubility and relatively high boiling point compared to other solvents. The iodine adsorption capacity (q) and removal efficiency ($E_{\%}$) were calculated using the following equations:

$$\text{Adsorption Capacity, q (mg/g)} = \frac{C_i - C_e}{M_S} \times V \quad (1)$$

$$\text{Removal Efficiency, } E_{\%} = \frac{C_i - C_e}{C_i} \times 100 \quad (2)$$

where C_i and C_e are the initial and the residual iodine concentrations in the solution (mg/L), V is the total volume of solution (L), and M_S is the adsorbent amount (g).

2.5. ADSORPTION ISOTHERM MODELS

Langmuir and Freundlich models were used to analyze and represent the iodine adsorption data. Langmuir isotherm model assumes that the surface of the adsorbent is covered with uniform homogeneous adsorption sites with a monolayer of adsorbed molecules, whereas Freundlich isotherm model is constructed on the assumptions of a multilayer adsorption with heterogeneous and non-uniform adsorption sites [29]. The Langmuir and Freundlich isotherm models can be mathematically expressed in the linear forms by Equation 3 and Equation 4, respectively

$$\frac{C_e}{Q_e} = \frac{1}{Q_{\max} K_L} + \frac{C_e}{Q_{\max}} \tag{3}$$

$$Log\left(Q_e\right) = Log\left(K_f\right) + \frac{Log\left(C_e\right)}{n} \tag{4}$$

where Q_e is the adsorption amount (mg/g), Q_{max} is the maximum adsorption capacity (mg/g), K_L is Langmuir constant (L/mg), K_f is Freundlich constant and n is Freundlich exponent.

3. RESULTS AND DISCUSSIONS

3.1. ADSORBENTS CHARACTERIZATION

N_2 physisorption isotherms were obtained for all the materials synthesized in this work. It is obvious, from Figure 1**,** that the isotherm of the materials follows type IV isotherm with an H1 hysteresis loop which is indicative of a mesoporous material. γ-Al_2O_3 shows higher N_2 uptake than the grafted samples due to the high porosity. Furthermore, it is also clear that the Al/DMAPS displayed a higher N_2 uptake than Al/APS and Al/MAPS.

The textural properties listed in Table1 showed that the material with the highest overall surface area was γ-Al_2O_3 (251 m^2/g). The surface area declined after grafting which is indicative of a successful grafting. Among the grafted adsorbents, Al/DMAPS (Table 1) had higher surface area than Al/APS and Al/MAPS. This was expected as Al/DMAPS had higher iodine adsorption capacities (Figure 1a). The pore size distribution (PSD) curves in Figure 1b showed a shift in pore size to a smaller values after grafting; however, the PSD for the grafted materials were uniform in the range of 10-11 nm.

Table 1.Textural properties of γ-Al_2O_3 before and after amine grafting.

Adsorbent	**S_{BET} (m^2/g)**	**V_p (cm^3/g)**	**D_p (nm)**
γ-Al_2O_3	251	1.030	12
Al/APS	163	0.312	11
Al/MAPS	167	0.474	10
Al/DMAPS	191	0.685	10

The FTIR spectra of γ-Al_2O_3, Al/APS, Al/MAPS, and Al/DMAPS were compared in the range of 4000-400 cm-1. Figure 3 shows a quintessential vibrational band for all samples except for a minor distinctions between them. The band at 3450 and 1620 cm^{-1} can be attributed to –OH stretching and H—O—H bending, respectively. The peaks at 510, 720 and 1050 cm^{-1} corresponds to the Al—O (AlO_6 octahedron), Al—O (AlO_4 tetrahedron) stretching and Al—OH bending, respectively. [30–32] Furthermore, the bands in 3050, 2930 and the 1600-1450 cm^{-1} range are all related to the C—N stretching, whereas the peaks in the 1400-1300 cm^{-1} range correspond to the N—O stretching [33–35]. The presence of a peak at 1460 cm^{-1} on the grafted samples spectra is associated with carbonate

species which was formulated by the attraction between the basic O^{2-} active sites and CO_2 [36]. The peaks in the range 1050-1225 and 2700-3050 cm^{-1} are present only in the grafted samples which is an indicative of successful aminosilane functionalization. After the iodine adsorption tests were finished, the iodine loaded sorbents were also studied by FTIR. Their spectra showed no chemical structural deformations. Furthermore, the vibrational bands at 3450, 3050, 1620 and 1460 cm^{-1} exhibited a noticeable increase which could be explained by the chemisorption phenomenon.

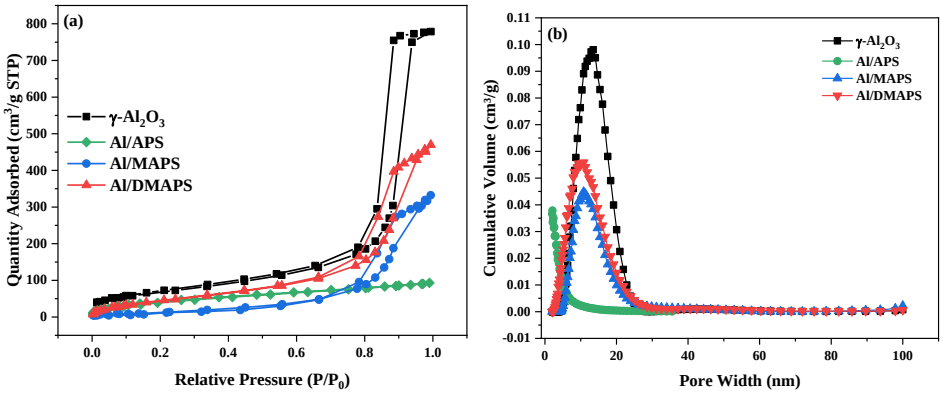

Figure 1. a) N2 physisorption isotherms and b) pore size distribution.

3.2. THE ADSORPTION OF IODINE ON AMINE-GRAFTED γ-Al_2O_3

The effect of different amines was investigated first to determine the best performing amine for iodine adsorption. The samples were tested for 24 h at 50 oC with 30% amine loading. The UV-Vis spectra of the iodine solution after the adsorption test are shown in Figure 4a where iodine in toluene display a peak at 498±3 nm. The absorbance peaks then were converted into adsorption capacities, shown in Figure 4b. The results showed that Al/DMAPS performed better and was able to remove 95% of the iodine with a capacity of 241 mg/g. Al/MAPS demonstrated a respectable performance with removal

efficiency of 87.7% and an iodine adsorption capacity of 223 mg/g. For the Al/APS sample, it had a poor performance with a removal efficiency of 51 % and iodine adsorption capacity of 124 mg/g. The result shows that the sample grafted with the tertiary amine had the highest capacity. It worth noting that the sample grafted with the secondary amine had a respectable performance. However, the sample grafted with the primary amine presented a weak adsorption capacity. These results proves that the branched amine has a positive effect on capacity. Furthermore, Al/DMAPS exhibited higher surface area than Al/MAPS and Al/APS (Table 1). Al/DMAPS was chosen to be tested on the following tests to get the optimal conditions for iodine adsorption from a liquid phase.

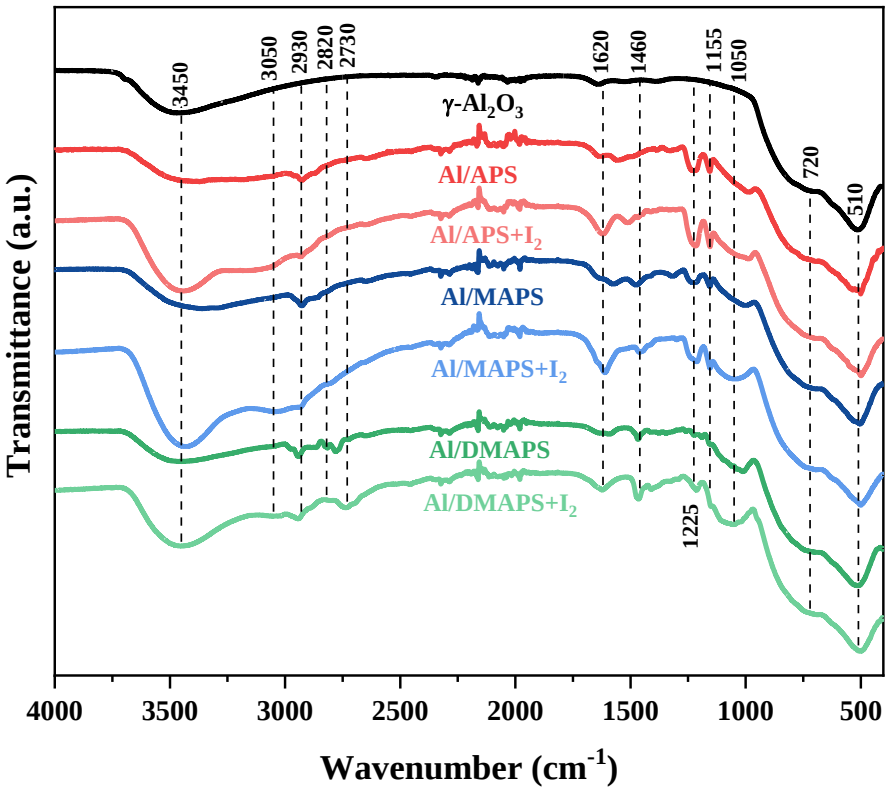

Figure 2. FTIR spectra for bare and amine-grafted alumina.

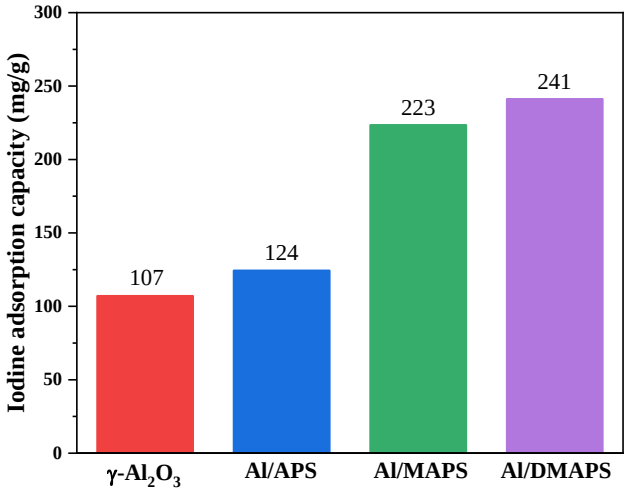

Figure 3. Iodine adsorption capacities at 50 oC after 24 h.

Next, the effect of temperature was studied. The sorbent Al/DMAPS was tested at 25, 50, and 80 ^{o}C to show the optimal adsorption temperature. It was found that the run at 80 ^{o}C showed the highest adsorption capacity (252 mg/g). Despite that, 50 ^{o}C is the optimal temperature because the amines functional groups are not thermally stable at high temperatures.

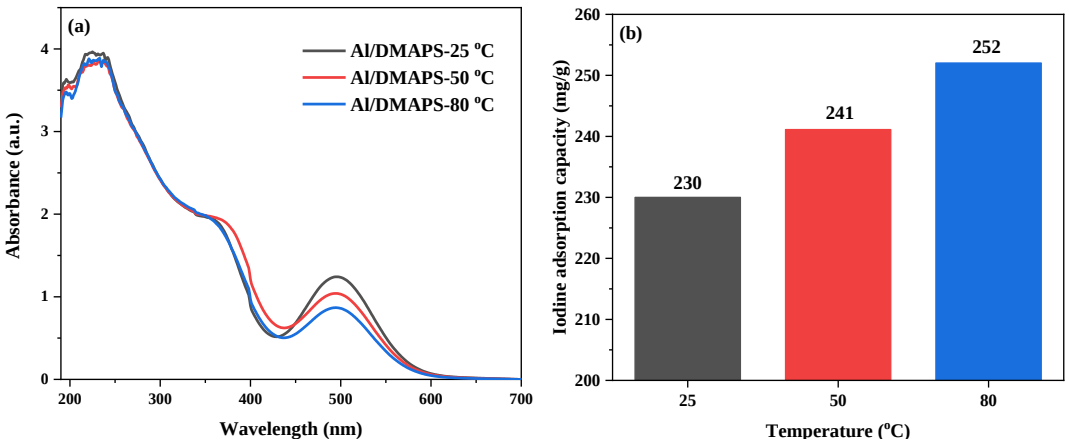

Figure 4. a)The UV-Vis spectrum viewing the effect of temperature on iodine adsorption via Al/DMAPS and b) shows the adsorption capacities.

The effect of amine loading was studied on Al/DMAPS (Figure 6a). Since all the grafted samples that were tested thus far were 30 wt% amine-loaded, 40 (40-Al/DMAPS) and 50 (50-Al/DMAPS) wt% samples were prepared. DMAPS was chosen for this test due to its superior adsorption capacity. 40-Al/DMAPS and 50-Al/DMAPS (Figure 6b) showed higher capacity than Al/DMAPS by 1.2 and 2.5%, respectively. The small increase in iodine capacity with higher amine loading is attributed to reaching the saturation limit of the mesoporous alumina.

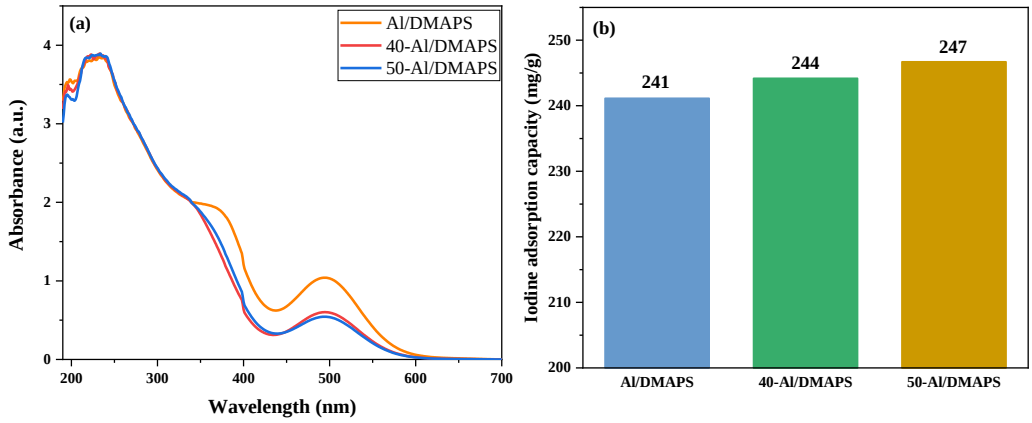

Figure 5. a) The UV-Vis spectrum showing the effect of DMAPS loading on iodine removal efficiency by at 50 ^{o}C and b) shows the capacities.

3.3. ADSORPTION ISOTHERM MODELS

Langmuir and Freundlich adsorption models were chosen to analyze the data obtained from the experimental work. The data from varying the initial iodine concentration test were used with the linear forms of the two models (Equation 3, Equation 4) to find the theoretical maximum iodine adsorption capacity at optimal conditions. For Langmuir model, C_e vs C_e/Q_e were plotted (Figure 7a) and the best fit was used to get the

slope and intercept. The slope was used to calculate Q_{max} which was 238 mg/g. With a calculated Q_{max} (238 mg/g) that almost matches the experimental (241 mg/g) and an R^2 value of 0.994, Langmuir model describes the adsorption behavior well.

For Freundlich model, Log(C_e) vs Log(Q_e) were drawn (Figure 7b) and the best fit was used to find the slope and intercept. The Freundlich constant, K_f, and exponent, n, were calculated and listed in Table 2 along with the Langmuir parameters. Noticeably, Freundlich model showed more variance (R^2 = 0.986); nonetheless, it still describes the behavior of iodine adsorption on Al/DMAPS rather well.

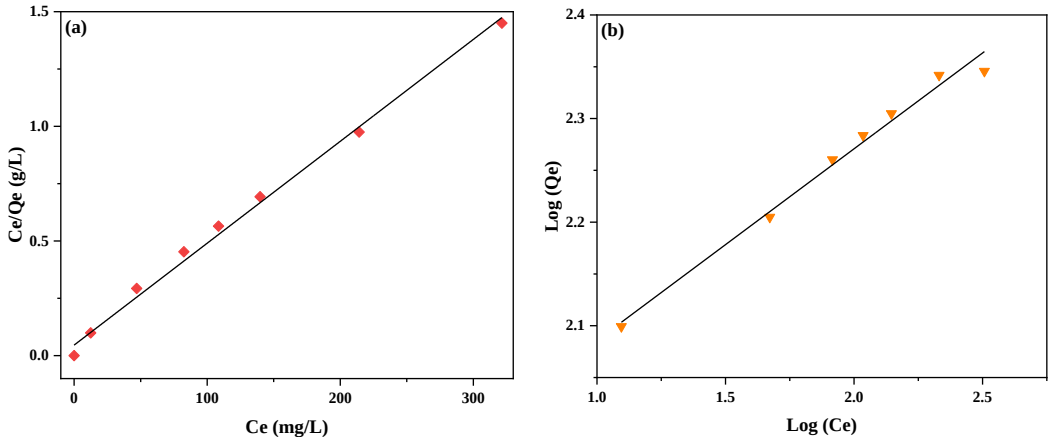

Figure 6. (a) Langmuir and (b) Freundlich models for iodine adsorption on Al/DMAPS.

Table 2. The parameters for Langmuir and Freundlich adsorption isotherm for iodine adsorption on Al/DMAPS.

	Langmuir			Freundlich		
$Q_{max\ Exp}$ (mg/g)*	Q_{max} (mg/g)	K_L (L/mg)	R^2	K_f	n	R^2
241	227	0.096	0.994	79.58	5.405	0.986

*Maximum experimental capacity.

4. CONCLUSIONS

In conclusion, mesoporous γ-Al_2O_3 was successfully grafted with three types of amines via class 2 technique. The synthesized adsorbents were then tested for RI removal from liquid phase, and reported an increase in the adsorption capacities for the grafted ones. The tertiary, secondary and primary amines showed higher adsorption capacities than the bare alumina by 125, 108, and 16%, respectively. Testing the effect of increasing the amine loading revealed that mesoporous alumina is close to saturation with amine because the capacities had minor gains. Despite the decrease in surface area, MAPS and DMAPS showed high affinity for I^-.

ACKNOWLEDGEMENTS

Mansour Alsalbokh would like to acknowledge Saudi Arabian Cultural Mission to the US (SACM) for their financial support.

REFERENCES

[1] De Ruysscher D, Niedermann G, Burnet N G, Siva S, Lee A W M and Hegi-Johnson F 2019 Radiotherapy toxicity Nat. Rev. Dis. Prim. 5

[2] Chapman N and Hooper A 2012 The disposal of radioactive wastes underground Proc. Geol. Assoc. 123 46–63

[3] Rußig S, Gonzalez V, Schurz M, Krzack S, Kleeberg J, Guhl S and Meyer B 2019 Particle residence time measurement in a pressurized drop-tube reactor with radioactive tracer Fuel 252 37–46

[4] Li K, Zhao Y, Zhang P, He C, Deng J, Ding S and Shi W 2016 Combined DFT and XPS investigation of iodine anions adsorption on the sulfur terminated (001) chalcopyrite surface Appl. Surf. Sci. 390 412–21

[5] Council N R, Studies D on E and L, Research B on R E and Incident and C to A the D and A of P I in the E of a N 2020 Distribution and Administration of Potassium Iodide in the Event of a Nuclear Incident Block Caving – A Viable Alternative? vol 21 (Washington D.C.: National Academies Press) pp 30–43

[6] Pei C, Ben T, Xu S and Qiu S 2014 Ultrahigh iodine adsorption in porous organic frameworks J. Mater. Chem. A 2 7179–87

[7] Sava Gallis D F, Ermanoski I, Greathouse J A, Chapman K W and Nenoff T M 2017 Iodine Gas Adsorption in Nanoporous Materials: A Combined Experiment-Modeling Study Ind. Eng. Chem. Res. 56 2331–8

[8] Wang H, Lustig W P and Li J 2018 Sensing and capture of toxic and hazardous gases and vapors by metal-organic frameworks Chem. Soc. Rev. 47 4729–56

[9] Azambre B and Chebbi M 2017 Evaluation of Silver Zeolites Sorbents Toward Their Ability to Promote Stable CH3I Storage as AgI Precipitates ACS Appl. Mater. Interfaces 9 25194–203

[10] Faghihian H, Maragheh M G and Malekpour A 2002 Adsorption of radioactive iodide by natural zeolites J. Radioanal. Nucl. Chem. 254 545–50

[11] Chibani S, Chebbi M, Lebègue S, Cantrel L and Badawi M 2016 Impact of the Si/Al ratio on the selective capture of iodine compounds in silver-mordenite: A periodic DFT study Phys. Chem. Chem. Phys. 18 25574–81

[12] Wu L, Sawada J A, Kuznicki D B, Kuznicki T and Kuznicki S M 2014 Iodine adsorption on silver-exchanged titania-derived adsorbents J. Radioanal. Nucl. Chem. 302 527–32

[13] Al-Mamoori A, Alsalbokh M, Lawson S, Rownaghi A A and Rezaei F 2019 Development of bismuth-mordenite adsorbents for iodine capture from off-gas streams Chem. Eng. J.

[14] Lefèvre G, Bessière J, Ehrhardt J J and Walcarius A 2003 Immobilization of iodide on copper(I) sulfide minerals J. Environ. Radioact. 70 73–83

[15] Hoskins J S, Karanfil T and Serkiz S M 2002 Removal and sequestration of iodide using silver-impregnated activated carbon Environ. Sci. Technol. 36 784–9

[16] Xu W, Zhang W, Kang J and Li B 2019 Facile synthesis of mesoporous Fe-based MOFs loading bismuth with high speed adsorption of iodide from solution J. Solid State Chem. 269 558–65

[17] Zhao X, Han X, Li Z, Huang H, Liu D and Zhong C 2015 Enhanced removal of iodide from water induced by a metal-incorporated porous metal-organic framework Appl. Surf. Sci. 351 760–4

[18] Bo A, Sarina S, Zheng Z, Yang D, Liu H and Zhu H 2013 Removal of radioactive iodine from water using Ag2O grafted titanate nanolamina as efficient adsorbent J. Hazard. Mater. 246–247 199–205

[19] Peng M and Wondraczek L 2009 Bismuth-doped oxide glasses as potential solar spectral converters and concentrators J. Mater. Chem. 19 627–30

[20] Yang J H, Cho Y J, Shin J M and Yim M S 2015 Bismuth-embedded SBA-15 mesoporous silica for radioactive iodine capture and stable storage J. Nucl. Mater. 465 556–64

[21] Kodama H 1992 Solidification of Iodide Ion by Reaction with Bi 2 O 3 Bull. Chem. Soc. Jpn. 65 3011–4

[22] Krzton-Maziopa A, Guguchia Z, Pomjakushina E, Pomjakushin V, Khasanov R, Luetkens H, Biswas P K, Amato A, Keller H and Conder K 2014 Superconductivity in a new layered bismuth oxyselenide: LaO 0.5F0.5BiSe2 J. Phys. Condens. Matter 26 1–6

[23] Han S, Um W and Kim W S 2019 Development of bismuth-functionalized graphene oxide to remove radioactive iodine Dalt. Trans. 48 478–85

[24] Liu S, Kang S, Wang H, Wang G, Zhao H and Cai W 2016 Nanosheets-built flowerlike micro/nanostructured Bi2O2.33 and its highly efficient iodine removal performances Chem. Eng. J. 289 219–30

[25] Zhang T, Yue X, Gao L, Qiu F, Xu J, Rong J and Pan J 2017 Hierarchically porous bismuth oxide/layered double hydroxide composites: Preparation, characterization and iodine adsorption J. Clean. Prod. 144 220–7

[26] Al-Mamoori A, Rownaghi A A and Rezaei F 2018 Combined Capture and Utilization of CO2 for Syngas Production over Dual-Function Materials ACS Sustain. Chem. Eng. 6 13551–61

[27] Lawson S, Griffin C, Rapp K, Rownaghi A A and Rezaei F 2019 Amine-Functionalized MIL-101 Monoliths for CO 2 Removal from Enclosed Environments Energy and Fuels 33 2399–407

[28] Gelles T, Lawson S, Rownaghi A A and Rezaei F 2020 Recent advances in development of amine functionalized adsorbents for CO2 capture vol 26 (Springer US)

[29] Kecili R and Mustansar Hussain C 2018 Chapter 4 - Mechanism of Adsorption on Nanomaterials pp 89–115

[30] Du X, Wang Y, Su X and Li J 2009 Influences of pH value on the microstructure and phase transformation of aluminum hydroxide Powder Technol. 192 40–6

[31] Gangwar J, Gupta B K, Tripathi S K and Srivastava A K 2015 Phase dependent thermal and spectroscopic responses of Al2O3 nanostructures with different morphogenesis Nanoscale 7 13313–44

[32] Shen L, Hu C, Sakka Y and Huang Q 2012 Study of phase transformation behaviour of alumina through precipitation method J. Phys. D. Appl. Phys. 45

[33] Rezaei F and Jones C W 2013 Stability of supported amine adsorbents to SO2 and NO x in postcombustion CO2 capture. 1. single-component adsorption Ind. Eng. Chem. Res. 52 12192–201

[34] Coates J 2004 Encyclopedia of Analytical Chemistry -IInterpretation of Infrared Spectra, A Practical Approach Encycl. Anal. Chem. 1–23

[35] Rezaei F, Sakwa-Novak M A, Bali S, Duncanson D M and Jones C W 2015 Shaping amine-based solid CO2 adsorbents: Effects of pelletization pressure on the physical and chemical properties Microporous Mesoporous Mater. 204 34–42

[36] Potter M E, Cho K M, Lee J J and Jones C W 2017 Role of Alumina Basicity in CO2 Uptake in 3-Aminopropylsilyl-Grafted Alumina Adsorbents ChemSusChem 10 2192–201

SECTION

3. CONCLUSIONS AND FUTURE OUTLOOK

3.1. CONCLUSIONS

Radioactive materials, specifically radioactive iodine, are serious problems facing humanity in the future with the spread of NPPs. Nuclear power generation is superior in term of efficiency and emissions and humans can control NNPs and tune them to perfection, but they cannot control natural disasters that can cause RI and other radionuclides to leak to the environment. RI can cause adverse health effects, like thyroid cancer, on humans. Furthermore, there are many pathways for RI to enter the body. One of them is through RI-contaminated irrigation water that leads to contaminated soil, which would lead to contaminated plantations. Adsorption techniques have been used for RI removal from both gas and liquid phases. Porous-organic frameworks and silver-based material technologies are the commonly used techniques for RI removal from the gas phase in the industry. For the liquid phase, metal-oxides and metal-oxides impregnated materials were studied extensively. Bismuth has been studied for replacing silver for its weak toxicity, low cost and adsorption performance. Furthermore, some amine groups have stronge affinities for iodine ions which, potentially, make grafting amines on the surface of the adsorbent promising for RI removal.

3.2. OUTLOOK

Mesoporous alumina has great potential for removing radionuclides from the liquid—water—phase, and this work is in its infancy. The next step in this work should be studying the sustainability and recyclability of grafted bismuth alumina and grafted bare alumina. In many of the papers reviewed in this work, surface modification techniques were employed to create strong affinity for iodine ions, hence the high iodine adsorption capacities. Some of these techniques, like using thiophene and pyridine, should be used with alumina. The natural progression of this work is to ultimately synthesize a product that is capable of removing iodine from a continuous flow system. Two methods can be suggested in this case which are 1) palletization, 2) 3D printed monoliths and 3) hollow fibers. Pellets or granular adsorbents have been continuously used in the industry and they are durable and easy to recycle or regenerate. In the last decade, 3D printed monoliths gained attention for their scalability, complex-shape channels, and channels tunability. Hollow fibers are promising new technology that should be studie

BIBLIOGRAPHY

[1] D. De Ruysscher, G. Niedermann, N.G. Burnet, S. Siva, A.W.M. Lee, F. Hegi-Johnson, Radiotherapy toxicity, Nat. Rev. Dis. Prim. 5 (2019). https://doi.org/10.1038/s41572-019-0064-5.

[2] N. Chapman, A. Hooper, The disposal of radioactive wastes underground, Proc. Geol. Assoc. 123 (2012) 46–63. https://doi.org/10.1016/j.pgeola.2011.10.001.

[3] S. Rußig, V. Gonzalez, M. Schurz, S. Krzack, J. Kleeberg, S. Guhl, B. Meyer, Particle residence time measurement in a pressurized drop-tube reactor with radioactive tracer, Fuel. 252 (2019) 37–46. https://doi.org/10.1016/j.fuel.2019.03.134.

[4] C. Pei, T. Ben, S. Xu, S. Qiu, Ultrahigh iodine adsorption in porous organic frameworks, J. Mater. Chem. A. 2 (2014) 7179–7187. https://doi.org/10.1039/c4ta00049h.

[5] K. Li, Y. Zhao, P. Zhang, C. He, J. Deng, S. Ding, W. Shi, Combined DFT and XPS investigation of iodine anions adsorption on the sulfur terminated (001) chalcopyrite surface, Appl. Surf. Sci. 390 (2016) 412–421. https://doi.org/10.1016/j.apsusc.2016.08.095.

[6] N.R. Council, D. on E. and L. Studies, B. on R.E. Research, and C. to A. the D. and A. of P.I. in the E. of a N. Incident, Distribution and Administration of Potassium Iodide in the Event of a Nuclear Incident, in: Block Caving – A Viable Altern., National Academies Press, Washington D.C., 2020: pp. 30–43.

[7] D.F. Sava Gallis, I. Ermanoski, J.A. Greathouse, K.W. Chapman, T.M. Nenoff, Iodine Gas Adsorption in Nanoporous Materials: A Combined Experiment-Modeling Study, Ind. Eng. Chem. Res. 56 (2017) 2331–2338. https://doi.org/10.1021/acs.iecr.6b04189.

[8] A. Smith, Norway Nuclear Reactor Leaks Radioactive Iodine: Officials, NBC News. (2016).

[9] Y. Wakatsuki, New radioactive water leak at Japan's Fukushima Daiichi plant, CNN. (2014).

[10] N. KARLINSKY, W. BRUNDIGE, L. TANGLAO, Japan Nuclear Crisis: Highest Radiation Levels Detected in Seawater, ABC News. (2011). https://abcnews.go.com/International/japan-nuclear-crisis-highest-radiation-levels-detected-seawater/story?id=13253117.

[11] M.R. Haymart, M. Banerjee, A.K. Stewart, R.J. Koenig, J.D. Birkmeyer, J.J. Griggs, Use of radioactive iodine for thyroid cancer, JAMA - J. Am. Med. Assoc. 306 (2011) 721–728. https://doi.org/10.1001/jama.2011.1139.

[12] Radioactive Iodine (Radioiodine) Therapy for Thyroid Cancer, Am. Cancer Soc. (2019). https://www.cancer.org/cancer/thyroid-cancer/treating/radioactive-iodine.html.

[13] B.. Rao, Genetic Hazards of X-Rays, 1958. https://doi.org/10.1056/nejm195802202580817.

[14] D. Darmawan, HEALTH CONSEQUENCES OF RADIATION EXPOSURE, in: J. Chem. Inf. Model., National Academies Press, 2004: pp. 44–67. https://doi.org/10.1017/CBO9781107415324.004.

[15] M.H. Choi, H.E. Shim, S.J. Yun, S.H. Park, D.S. Choi, B.S. Jang, Y.J. Choi, J. Jeon, Gold-Nanoparticle-Immobilized Desalting Columns for Highly Efficient and Specific Removal of Radioactive Iodine in Aqueous Media, ACS Appl. Mater. Interfaces. 8 (2016) 29227–29231. https://doi.org/10.1021/acsami.6b11136.

[16] M.E. Potter, K.M. Cho, J.J. Lee, C.W. Jones, Role of Alumina Basicity in CO2 Uptake in 3-Aminopropylsilyl-Grafted Alumina Adsorbents, ChemSusChem. 10 (2017) 2192–2201. https://doi.org/10.1002/cssc.201700115.

[17] M.A. Sakwa-Novak, C.J. Yoo, S. Tan, F. Rashidi, C.W. Jones, Poly(ethylenimine)-Functionalized Monolithic Alumina Honeycomb Adsorbents for CO2 Capture from Air, ChemSusChem. 9 (2016) 1859–1868. https://doi.org/10.1002/cssc.201600404.

[18] W. Chaikittisilp, H.J. Kim, C.W. Jones, Mesoporous alumina-supported amines as potential steam-stable adsorbents for capturing CO2 from simulated flue gas and ambient air, Energy and Fuels. 25 (2011) 5528–5537. https://doi.org/10.1021/ef201224v.

[19] S. Bali, J. Leisen, G.S. Foo, C. Sievers, C.W. Jones, Aminosilanes grafted to basic alumina as CO2 adsorbents-role of grafting conditions on CO2 adsorption properties, ChemSusChem. 7 (2014) 3145–3156. https://doi.org/10.1002/cssc.201402373.

[20] F. Rezaei, M.A. Sakwa-Novak, S. Bali, D.M. Duncanson, C.W. Jones, Shaping amine-based solid CO2 adsorbents: Effects of pelletization pressure on the physical and chemical properties, Microporous Mesoporous Mater. 204 (2015) 34–42. https://doi.org/10.1016/j.micromeso.2014.10.047.

[21] D.W. Kolpin, E.T. Furlong, M.T. Meyer, E.M. Thurman, S.D. Zaugg, L.B. Barber, H.T. Buxton, Pharmaceuticals, hormones, and other organic wastewater contaminants in U.S. streams, 1999-2000: A national reconnaissance, Environ. Sci. Technol. 36 (2002) 1202–1211. https://doi.org/10.1021/es011055j.

[22] S.C. Lee, M.S. Cho, S.Y. Jung, C.K. Ryu, J.C. Kim, Effects of alumina phases on CO2 sorption and regeneration properties of potassium-based alumina sorbents, Adsorption. 20 (2014) 331–339. https://doi.org/10.1007/s10450-013-9596-2.

[23] L. Kovarik, M. Bowden, D. Shi, N.M. Washton, A. Andersen, J.Z. Hu, J. Lee, J. Szanyi, J.H. Kwak, C.H.F. Peden, Unraveling the Origin of Structural Disorder in High Temperature Transition Al2O3: Structure of θ-Al2O3, Chem. Mater. 27 (2015) 7042–7049. https://doi.org/10.1021/acs.chemmater.5b02523.

[24] L. Kovarik, M. Bowden, A. Genc, J. Szanyi, C.H.F. Peden, J.H. Kwak, Structure of δ-alumina: Toward the atomic level understanding of transition alumina phases, J. Phys. Chem. C. 118 (2014) 18051–18058. https://doi.org/10.1021/jp500051j.

[25] I. Levin, D. Brandon, Metastable alumina polymorphs: Crystal structures and transition sequences, J. Am. Ceram. Soc. 81 (1998) 1995–2012. https://doi.org/10.1111/j.1151-2916.1998.tb02581.x.

[26] I.A. Leenson, Sublimation of iodine at various pressures. Multipurpose experiments in inorganic and physical chemistry, J. Chem. Educ. 82 (2005) 241–245. https://doi.org/10.1021/ed082p241.

[27] D.I. Kaplan, S. Zhang, K.A. Roberts, K. Schwehr, C. Xu, D. Creeley, Y.F. Ho, H.P. Li, C.M. Yeager, P.H. Santschi, Radioiodine concentrated in a wetland, J. Environ. Radioact. 131 (2014) 57–61. https://doi.org/10.1016/j.jenvrad.2013.09.001.

[28] F.X. Llabrés i Xamena, A. Abad, A. Corma, H. Garcia, MOFs as catalysts: Activity, reusability and shape-selectivity of a Pd-containing MOF, J. Catal. 250 (2007) 294–298. https://doi.org/10.1016/j.jcat.2007.06.004.

[29] Z.J. Lin, J. Lü, M. Hong, R. Cao, Metal-organic frameworks based on flexible ligands (FL-MOFs): Structures and applications, Chem. Soc. Rev. 43 (2014) 5867–5895. https://doi.org/10.1039/c3cs60483g.

[30] K.K. Gangu, S. Maddila, S.B. Mukkamala, S.B. Jonnalagadda, Synthesis, Structure, and Properties of New Mg(II)-Metal-Organic Framework and Its Prowess as Catalyst in the Production of 4H-Pyrans, Ind. Eng. Chem. Res. 56 (2017) 2917–2924. https://doi.org/10.1021/acs.iecr.6b04795.

[31] D. Sheberla, J.C. Bachman, J.S. Elias, C.J. Sun, Y. Shao-Horn, M. Dincă, Conductive MOF electrodes for stable supercapacitors with high areal capacitance, Nat. Mater. 16 (2017) 220–224. https://doi.org/10.1038/nmat4766.

[32] Q. Al-Naddaf, M. Al-Mansour, H. Thakkar, F. Rezaei, MOF-GO Hybrid Nanocomposite Adsorbents for Methane Storage, Ind. Eng. Chem. Res. 57 (2018) 17470–17479. https://doi.org/10.1021/acs.iecr.8b03638.

[33] S. Lawson, M. Snarzyk, D. Hanify, A.A. Rownaghi, F. Rezaei, Development of 3D-Printed Polymer-MOF Monoliths for CO2 Adsorption, Ind. Eng. Chem. Res. (2019). https://doi.org/10.1021/acs.iecr.9b05445.

[34] S. Lawson, C. Griffin, K. Rapp, A.A. Rownaghi, F. Rezaei, Amine-Functionalized MIL-101 Monoliths for CO 2 Removal from Enclosed Environments, Energy and Fuels. 33 (2019) 2399–2407. https://doi.org/10.1021/acs.energyfuels.8b04508.

[35] D.F. Sava, K.W. Chapman, M.A. Rodriguez, J.A. Greathouse, P.S. Crozier, H. Zhao, P.J. Chupas, T.M. Nenoff, Competitive I2 sorption by Cu-BTC from humid gas streams, Chem. Mater. 25 (2013) 2591–2596. https://doi.org/10.1021/cm401762g.

[36] Z. Yan, Y. Yuan, Y. Tian, D. Zhang, G. Zhu, Highly efficient enrichment of volatile iodine by charged porous aromatic frameworks with three sorption sites, Angew. Chemie - Int. Ed. 54 (2015) 12733–12737. https://doi.org/10.1002/anie.201503362.

[37] S. Qiao, W. Huang, Z. Du, X. Chen, F.K. Shieh, R. Yang, Phosphine oxide-based conjugated microporous polymers with excellent CO2 capture properties, New J. Chem. 39 (2015) 136–141. https://doi.org/10.1039/c4nj01477d.

[38] F. Ren, Z. Zhu, X. Qian, W. Liang, P. Mu, H. Sun, J. Liu, A. Li, Novel thiophene-bearing conjugated microporous polymer honeycomb-like porous spheres with ultrahigh iodine uptake, Chem. Commun. 52 (2016) 9797–9800. https://doi.org/10.1039/c6cc05188j.

[39] K. Su, W. Wang, B. Li, D. Yuan, Azo-Bridged Calix[4]resorcinarene-Based Porous Organic Frameworks with Highly Efficient Enrichment of Volatile Iodine, ACS Sustain. Chem. Eng. 6 (2018) 17402–17409. https://doi.org/10.1021/acssuschemeng.8b05203.

[40] X. Guo, Y. Tian, M. Zhang, Y. Li, R. Wen, X. Li, X. Li, Y. Xue, L. Ma, C. Xia, S. Li, Mechanistic Insight into Hydrogen-Bond-Controlled Crystallinity and Adsorption Property of Covalent Organic Frameworks from Flexible Building Blocks, Chem. Mater. 30 (2018) 2299–2308. https://doi.org/10.1021/acs.chemmater.7b05121.

[41] T. Geng, C. Zhang, M. Liu, C. Hu, G. Chen, Preparation of biimidazole-based porous organic polymers for ultrahigh iodine capture and formation of liquid complexes with iodide/polyiodide ions, J. Mater. Chem. A. 8 (2020) 2820–2826. https://doi.org/10.1039/c9ta11982e.

[42] H. Wang, W.P. Lustig, J. Li, Sensing and capture of toxic and hazardous gases and vapors by metal-organic frameworks, Chem. Soc. Rev. 47 (2018) 4729–4756. https://doi.org/10.1039/c7cs00885f.

[43] B. Azambre, M. Chebbi, Evaluation of Silver Zeolites Sorbents Toward Their Ability to Promote Stable CH3I Storage as AgI Precipitates, ACS Appl. Mater. Interfaces. 9 (2017) 25194–25203. https://doi.org/10.1021/acsami.7b02366.

[44] H. Faghihian, M.G. Maragheh, A. Malekpour, Adsorption of radioactive iodide by natural zeolites, J. Radioanal. Nucl. Chem. 254 (2002) 545–550. https://doi.org/10.1023/A:1021698207045.

[45] H. Jabraoui, E.P. Hessou, S. Chibani, L. Cantrel, S. Lebègue, M. Badawi, Adsorption of volatile organic and iodine compounds over silver-exchanged mordenites: A comparative periodic DFT study for several silver loadings, Appl. Surf. Sci. 485 (2019) 56–63. https://doi.org/10.1016/j.apsusc.2019.03.282.

[46] T.M. Nenoff, M.A. Rodriguez, N.R. Soelberg, K.W. Chapman, Silver-mordenite for radiologic gas capture from complex streams: Dual catalytic CH3I decomposition and I confinement, Microporous Mesoporous Mater. 200 (2014) 297–303. https://doi.org/10.1016/j.micromeso.2014.04.041.

[47] K.W. Chapman, P.J. Chupas, T.M. Nenoff, Radioactive iodine capture in silver-containing mordenites through nanoscale silver iodide formation, J. Am. Chem. Soc. 132 (2010) 8897–8899. https://doi.org/10.1021/ja103110y.

[48] M. Chebbi, S. Chibani, J.F. Paul, L. Cantrel, M. Badawi, Evaluation of volatile iodine trapping in presence of contaminants: A periodic DFT study on cation exchanged-faujasite, Microporous Mesoporous Mater. 239 (2017) 111–122. https://doi.org/10.1016/j.micromeso.2016.09.047.

[49] S. Chibani, M. Chebbi, S. Lebègue, L. Cantrel, M. Badawi, Impact of the Si/Al ratio on the selective capture of iodine compounds in silver-mordenite: A periodic DFT study, Phys. Chem. Chem. Phys. 18 (2016) 25574–25581. https://doi.org/10.1039/c6cp05015h.

[50] L. Wu, J.A. Sawada, D.B. Kuznicki, T. Kuznicki, S.M. Kuznicki, Iodine adsorption on silver-exchanged titania-derived adsorbents, J. Radioanal. Nucl. Chem. 302 (2014) 527–532. https://doi.org/10.1007/s10967-014-3252-5.

[51] A. Al-Mamoori, M. Alsalbokh, S. Lawson, A.A. Rownaghi, F. Rezaei, Development of bismuth-mordenite adsorbents for iodine capture from off-gas streams, Chem. Eng. J. (2019). https://doi.org/10.1016/j.cej.2019.123583.

[52] M. Peng, L. Wondraczek, Bismuth-doped oxide glasses as potential solar spectral converters and concentrators, J. Mater. Chem. 19 (2009) 627–630. https://doi.org/10.1039/b812316k.

[53] J.H. Yang, Y.J. Cho, J.M. Shin, M.S. Yim, Bismuth-embedded SBA-15 mesoporous silica for radioactive iodine capture and stable storage, J. Nucl. Mater. 465 (2015) 556–564. https://doi.org/10.1016/j.jnucmat.2015.06.043.

[54] H. Kodama, Solidification of Iodide Ion by Reaction with Bi 2 O 3 , Bull. Chem. Soc. Jpn. 65 (1992) 3011–3014. https://doi.org/10.1246/bcsj.65.3011.

[55] A. Krzton-Maziopa, Z. Guguchia, E. Pomjakushina, V. Pomjakushin, R. Khasanov, H. Luetkens, P.K. Biswas, A. Amato, H. Keller, K. Conder, Superconductivity in a new layered bismuth oxyselenide: LaO 0.5F0.5BiSe2, J. Phys. Condens. Matter. 26 (2014) 1–6. https://doi.org/10.1088/0953-8984/26/21/215702.

[56] J.L. Krumhansl, T.M. Nenoff, Hydrotalcite-like layered bismuth-iodine-oxides as waste forms, Appl. Geochemistry. 26 (2011) 57–64. https://doi.org/10.1016/j.apgeochem.2010.11.003.

[57] B.J. Riley, J.D. Vienna, D.M. Strachan, J.S. McCloy, J.L. Jerden, Materials and processes for the effective capture and immobilization of radioiodine: A review, J. Nucl. Mater. 470 (2016) 307–326. https://doi.org/10.1016/j.jnucmat.2015.11.038.

[58] G. Lefèvre, J. Bessière, J.J. Ehrhardt, A. Walcarius, Immobilization of iodide on copper(I) sulfide minerals, J. Environ. Radioact. 70 (2003) 73–83. https://doi.org/10.1016/S0265-931X(03)00119-X.

[59] J.S. Hoskins, T. Karanfil, S.M. Serkiz, Removal and sequestration of iodide using silver-impregnated activated carbon, Environ. Sci. Technol. 36 (2002) 784–789. https://doi.org/10.1021/es010972m.

[60] W. Xu, W. Zhang, J. Kang, B. Li, Facile synthesis of mesoporous Fe-based MOFs loading bismuth with high speed adsorption of iodide from solution, J. Solid State Chem. 269 (2019) 558–565. https://doi.org/10.1016/j.jssc.2018.10.028.

[61] X. Zhao, X. Han, Z. Li, H. Huang, D. Liu, C. Zhong, Enhanced removal of iodide from water induced by a metal-incorporated porous metal-organic framework, Appl. Surf. Sci. 351 (2015) 760–764. https://doi.org/10.1016/j.apsusc.2015.05.186.

[62] A. Bo, S. Sarina, Z. Zheng, D. Yang, H. Liu, H. Zhu, Removal of radioactive iodine from water using Ag2O grafted titanate nanolamina as efficient adsorbent, J. Hazard. Mater. 246–247 (2013) 199–205. https://doi.org/10.1016/j.jhazmat.2012.12.008.

[63] S. Liu, S. Kang, H. Wang, G. Wang, H. Zhao, W. Cai, Nanosheets-built flowerlike micro/nanostructured Bi2O2.33 and its highly efficient iodine removal performances, Chem. Eng. J. 289 (2016) 219–230. https://doi.org/10.1016/j.cej.2015.12.101.

[64] T. Zhang, X. Yue, L. Gao, F. Qiu, J. Xu, J. Rong, J. Pan, Hierarchically porous bismuth oxide/layered double hydroxide composites: Preparation, characterization and iodine adsorption, J. Clean. Prod. 144 (2017) 220–227. https://doi.org/10.1016/j.jclepro.2017.01.030.

[65] S. Han, W. Um, W.S. Kim, Development of bismuth-functionalized graphene oxide to remove radioactive iodine, Dalt. Trans. 48 (2019) 478–485. https://doi.org/10.1039/C8DT03745K.

[66] M.I. Hossain, A. Udoh, B.E. Grabicka, K.S. Walton, S.M.C. Ritchie, T.G. Glover, Membrane-Coated UiO-66 MOF Adsorbents, Ind. Eng. Chem. Res. 58 (2019) 1352–1362. https://doi.org/10.1021/acs.iecr.8b05275.

[67] N.C. Burtch, H. Jasuja, K.S. Walton, Water stability and adsorption in metal-organic frameworks, Chem. Rev. 114 (2014) 10575–10612. https://doi.org/10.1021/cr5002589.

[68] Z. Wang, Y. Huang, J. Yang, Y. Li, Q. Zhuang, J. Gu, The water-based synthesis of chemically stable Zr-based MOFs using pyridine-containing ligands and their exceptionally high adsorption capacity for iodine, Dalt. Trans. 46 (2017) 7412–7420. https://doi.org/10.1039/c7dt01084b.

[69] H. Li, Y. Li, B. Li, D. Liu, Y. Zhou, Highly selective anchoring silver nanoclusters on MOF/SOF heterostructured framework for efficient adsorption of radioactive iodine from aqueous solution, Chemosphere. 252 (2020). https://doi.org/10.1016/j.chemosphere.2020.126448.

[70] T. Gelles, S. Lawson, A.A. Rownaghi, F. Rezaei, Recent advances in development of amine functionalized adsorbents for CO2 capture, Springer US, 2020. https://doi.org/10.1007/s10450-019-00151-0.

[71] A. Al-Mamoori, A.A. Rownaghi, F. Rezaei, Combined Capture and Utilization of CO2 for Syngas Production over Dual-Function Materials, ACS Sustain. Chem. Eng. 6 (2018) 13551–13561. https://doi.org/10.1021/acssuschemeng.8b03769.

[72] C. Chen, W.S. Ahn, CO 2 capture using mesoporous alumina prepared by a sol-gel process, Chem. Eng. J. 166 (2011) 646–651. https://doi.org/10.1016/j.cej.2010.11.038.

[73] A. Al-Mamoori, H. Thakkar, X. Li, A.A. Rownaghi, F. Rezaei, Development of Potassium- and Sodium-Promoted CaO Adsorbents for CO2 Capture at High Temperatures, Ind. Eng. Chem. Res. 56 (2017) 8292–8300. https://doi.org/10.1021/acs.iecr.7b01587.

[74] N. Science, R. January, Separation Technology for Radioactive Iodine from Off-Gas Streams of Nuclear Facilities, 1083 (1994) 1073–1083. https://doi.org/https://doi.org/10.3327/jnst.31.1073.

[75] M. V. Wilkinson, A. V. Mondino, A.C. Manzini, Separation of iodine produced from fission using silver-coated alumina, J. Radioanal. Nucl. Chem. 256 (2003) 413–415. https://doi.org/10.1023/A:1024583212400.

[76] Q.H. Cheng, Z.J. Li, T.W. Chu, Adsorption of gaseous iodine-131 at high temperatures by silver impregnated alumina, Nucl. Sci. Tech. 26 (2015) 1–5. https://doi.org/10.13538/j.1001-8042/nst.26.040303.

[77] A. Horvath, E. Rachlew, Nuclear power in the 21st century: Challenges and possibilities, Ambio. 45 (2016) 38–49. https://doi.org/10.1007/s13280-015-0732-y.

[78] K. Jie, Y. Zhou, E. Li, Z. Li, R. Zhao, F. Huang, Reversible Iodine Capture by Nonporous Pillar[6]arene Crystals, J. Am. Chem. Soc. 139 (2017) 15320–15323. https://doi.org/10.1021/jacs.7b09850.

[79] R. Kecili, C. Mustansar Hussain, Chapter 4 - Mechanism of Adsorption on Nanomaterials, in: 2018: pp. 89–115.

[80] X. Du, Y. Wang, X. Su, J. Li, Influences of pH value on the microstructure and phase transformation of aluminum hydroxide, Powder Technol. 192 (2009) 40–46. https://doi.org/10.1016/j.powtec.2008.11.008.

[81] J. Gangwar, B.K. Gupta, S.K. Tripathi, A.K. Srivastava, Phase dependent thermal and spectroscopic responses of Al2O3 nanostructures with different morphogenesis, Nanoscale. 7 (2015) 13313–13344. https://doi.org/10.1039/c5nr02369f.

[82] L. Shen, C. Hu, Y. Sakka, Q. Huang, Study of phase transformation behaviour of alumina through precipitation method, J. Phys. D. Appl. Phys. 45 (2012). https://doi.org/10.1088/0022-3727/45/21/215302.

[83] F. Rezaei, C.W. Jones, Stability of supported amine adsorbents to SO2 and NO x in postcombustion CO2 capture. 1. single-component adsorption, Ind. Eng. Chem. Res. 52 (2013) 12192–12201. https://doi.org/10.1021/ie4019116.

[84] J. Coates, Encyclopedia of Analytical Chemistry -IInterpretation of Infrared Spectra, A Practical Approach, Encycl. Anal. Chem. (2004) 1–23. http://www3.uma.pt/jrodrigues/disciplinas/QINO-II/Teorica/IR.pdf.

VITA

Mansour Mohammed Alsalbokh received his Bachelor of Science degree in Chemical Engineering from King Fahad University of Science and Minerals (KFUPM), Dhahran, Saudi Arabia in May 2016. Mansour received his scholarship from Saudi Arabian Cultural Mission (SACM) in Saudi Arabia to study for the master's degree in chemical engineering. He started at Missouri University of Science and Technology in the fall semester of 2018 and in spring 2019 he started working under the supervision of Dr. Ali Rownaghi. He received his Master of Science degree in Chemical Engineering from Missouri University of Science and Technology in December 2020